

NLO QCD+EW predictions for tHj and tZj production at the LHC

Davide Pagani^{*1}, Ioannis Tsinikos^{†2}, and Eleni Vryonidou^{‡3}

¹DESY, Theory Group, Notkestrasse 85, 22607 Hamburg, Germany

²Theoretical Particle Physics, Department of Astronomy and Theoretical Physics, Lund University, Sölvegatan 14A, SE-223 62 Lund, Sweden

³Theoretical Physics Department, CERN, CH-1211 Geneva 23, Switzerland

Abstract

In this work we calculate the cross sections for the hadroproduction of a single top quark or antiquark in association with a Higgs (tHj) or Z boson (tZj) at NLO QCD+EW accuracy. In the case of tZj production we consider both the case of the Z boson undecayed and the complete final state $t\ell^+\ell^-j$, including off-shell and non-resonant effects. We perform our calculation in the five-flavour-scheme (5FS), without selecting any specific production channel (s -, t - or tW associated). Moreover, we provide a more realistic estimate of the theory uncertainty by carefully including the differences between the four-flavour-scheme (4FS) and 5FS predictions. The difficulties underlying this procedure in the presence of EW corrections are discussed in detail. We find that NLO EW corrections are in general within the NLO QCD theory uncertainties only if the flavour scheme uncertainty (4FS vs. 5FS) is taken into account. For the case of $t\ell^+\ell^-j$ production we also investigate differences between NLO QCD+EW predictions and NLO QCD predictions matched with a parton shower simulation including multiple photon emissions.

1 Introduction

The study of the interactions of the top quark, gauge and Higgs bosons is one of the main goals of TeV-scale colliders. After the discovery of the Higgs boson in the Run I, the Large Hadron Collider (LHC) has reached a golden era of precision physics and will continue to stress-test the predictions of the Standard Model (SM) of elementary particles. The success of this ambitious research program critically depends on a collaborative theoretical and experimental effort to detect deviations and/or constrain new physics, with sensitivities that reach the multi-TeV scale. The LHC has opened new possibilities, allowing for the first time the measurement of processes that directly probe the interaction of the top quark with both the neutral gauge bosons and the Higgs boson. This set of processes consists of the associated production of a single top or a top-quark pair with a Higgs or a neutral gauge boson. Since these processes probe some of the least known interactions in the SM, they have attracted considerable attention both on the experimental and theoretical side. The leading production mechanism for top-pair

*davide.pagani@desy.de

†ioannis.tsinikos@thep.lu.se

‡eleni.vryonidou@cern.ch

associated production is through QCD interactions (at order $\alpha_s^2\alpha$ at the Born level). Single top associated production, which is the focus of this work, proceeds instead via electroweak interactions. Whilst single top production (tj) has only a rate of roughly one third of the strong $t\bar{t}$ production, tZj has a cross section similar to the $t\bar{t}Z$ one. Indeed, single top production in association with a Z boson has already been measured at the LHC by both CMS [1, 2] and ATLAS [3, 4]. Finally the tHj rate is about 10% of the $t\bar{t}H$ one, and the process has been searched for at the LHC [5–7].

The fact that this set of processes plays an important role in the search for new top-quark interactions has been studied extensively by the theory community [8–11]. They open up a unique possibility of probing top-Higgs, top-gauge, triple-gauge, gauge-Higgs interactions in the same final state. The complete analysis of the tZj and tHj processes in the Standard Model Effective Field Theory (SMEFT) framework, including next-to-leading (NLO) QCD corrections, was presented in Ref. [12]. This work demonstrated the importance of single top associated production as a probe of new interactions, and showed the crucial role these processes can play in a global SMEFT interpretation of top couplings. Another important finding was that differential distributions can be particularly sensitive to modifications of the top-quark interactions, therefore differential measurements of these processes can prove highly beneficial in constraining new physics effects.

The special role of single top associated production as a probe of new interactions as well as the increasing precision of the experimental inclusive measurements and the prospect of differential measurements demand a precise theoretical description of these processes within the Standard Model. This class of processes are “purely” electroweak, with the consequence that the QCD corrections are typically small and under control. The SM predictions at NLO in QCD for tZj and tHj were first presented in Refs. [13] and [11], respectively. Whilst Ref. [11] performs a detailed comparison between the four flavour scheme (4FS) and five flavour scheme (5FS) computations for tHj at both the inclusive and differential level, a corresponding exploration of the tZj process is lacking.

Motivated by the increasing precision of experimental measurements, the main goal of this paper is to revisit single top associated production within the SM, computing for the first time NLO QCD+EW corrections in the 5FS and examining the impact of higher-order corrections at both the inclusive and differential level for tHj , tZj and more in general $t\ell^+\ell^-j$ production. As a matter of fact, the results of our calculation correspond to one of the items of the 2019 Les Houches precision Standard Model wish list [14]. Moreover, similarly to Ref. [11], we perform a detailed comparison between the 4FS and 5FS computations and we design a strategy for taking into account their differences as an additional uncertainty, together with scale uncertainties and EW corrections. In the case of $t\ell^+\ell^-j$ production, where two leptons are present in the final state, we also compare NLO QCD+EW predictions at fixed order with NLO QCD predictions matched with parton shower effects including QED photon emissions from fermions.

This paper is organised as follows. In Sec. 2 we describe in detail our calculation setup. First, in Sec. 2.1, we discuss the differences between the 4FS and 5FS and we explain the strategy we have designed for taking into account their differences. In Sec. 2.2 we discuss the technical difficulties for separating t -, s - and tW associated modes when EW corrections are calculated, which partly motivate the aforementioned strategy. Input parameters are specified in Sec. 2.3. In Sec. 3 we provide and comment on numerical results obtained within MADGRAPH5_AMC@NLO [15, 16] and corresponding to the most precise predictions for tHj , tZj and $t\ell^+\ell^-j$ production to-date. In Sec. 3.1 we provide the predictions for total cross sections at NLO QCD+EW accuracy, while differential distributions are analysed in Sec. 3.2. In Sec. 3.3 we focus on the $t\ell^+\ell^-j$ process and discuss the differences between the fixed-order result at NLO QCD+EW accuracy and the NLO QCD prediction matched with a parton shower taking into account multiple photon emissions from fermions. We give our conclusions and

outlook in Sec. 4.

2 Calculation Setup

In this section we describe the calculation setup, which is common for the three processes considered in this work:

- $pp \longrightarrow tHj + \bar{t}Hj$,
- $pp \longrightarrow tZj + \bar{t}Zj$,
- $pp \longrightarrow t\ell^+\ell^-j + \bar{t}\ell^+\ell^-j$.

In the following, unless it is differently specified, with the notation tHj , tZj and $t\ell^+\ell^-j$ we will understand both the final states with top quarks and antiquarks. We remind the reader that the production process $t\ell^+\ell^-j$ corresponds to the production process tZj only in the limit $m(\ell^+\ell^-) \longrightarrow m_Z$, *i.e.*, in the narrow-width approximation. In general, off-shell and interference effects are present, especially, the $\ell^+\ell^-$ pair can also stem from an off-shell photon.

We calculate cross sections, at the inclusive and differential level, at NLO QCD+EW accuracy in the 5FS. Expanding in powers of α_s and α and following the notation already used in Refs. [16–24], the different contributions to any differential or inclusive cross section Σ can be denoted as:

$$\begin{aligned} \Sigma_{\text{LO}}(\alpha_s, \alpha) &= \alpha^{3+k} \Sigma_{3+k,0} \\ &\equiv \text{LO}_1, \end{aligned} \tag{1}$$

$$\begin{aligned} \Sigma_{\text{NLO}}(\alpha_s, \alpha) &= \alpha_s \alpha^{3+k} \Sigma_{4+k,0} + \alpha^{4+k} \Sigma_{4+k,1} \\ &\equiv \text{NLO}_1 + \text{NLO}_2, \end{aligned} \tag{2}$$

where $k = 0$ for tHj and tZj and $k = 1$ for $t\ell^+\ell^-j$. For convenience, we will also use the standard notation NLO_{QCD} and $\text{NLO}_{\text{QCD+EW}}$ for denoting the quantities $\text{LO}_1 + \text{NLO}_1$ and $\text{LO}_1 + \text{NLO}_1 + \text{NLO}_2$, respectively. In other words, the NLO_1 and NLO_2 terms are the NLO QCD and NLO EW corrections, respectively. One should note that no additional perturbative orders are present when all possible SM tree-level and one-loop diagrams contributing to these processes are taken into account. In other words, the complete-NLO, *i.e.* the set of all the possible contributions of $\mathcal{O}(\alpha_s^n \alpha^m)$ with $m, n > 0$ and $m + n \leq 4 + k$, and $\text{NLO}_{\text{QCD+EW}}$ predictions coincide. Similarly, the LO_1 contribution coincides with the LO prediction.¹ We note here that this is not the case for other relevant processes in top-quark physics, such as, *e.g.*, $t\bar{t}W$ and $t\bar{t}t\bar{t}$ for which the two approximations are different and lead to sizeable numerical differences due to contributions that are formally suppressed w.r.t. the NLO_{EW} in the (α_s/α) power counting [22, 23, 25, 26].

2.1 Flavour-scheme and scale uncertainties

As can be seen in Eq. (1), LO predictions do not depend on α_s ; for purely electroweak processes the dependence on α_s enters only via the NLO QCD corrections, the NLO_1 contribution in Eq. (2), or higher-order terms in the perturbative expansion. For this reason, while the explicit

¹These statements would not hold true in the 4FS, unless photon-initiated processes are artificially neglected. Indeed, any b -initiated contribution of order $\alpha_s^n \alpha^m$ in the 5FS is related to a corresponding gluon-initiated contribution of order $\alpha_s^{n+1} \alpha^m$ in the 4FS, via the $g \longrightarrow b\bar{b}$ splitting. However, it is also related to a corresponding photon-initiated contribution of order $\alpha_s^n \alpha^{n+1}$, via the $\gamma \longrightarrow b\bar{b}$ splitting. Therefore, following the notation already used in Refs. [16–24], also an LO_2 and an NLO_3 term would be present.

dependence on the factorisation scale μ_F is present already at LO, the explicit dependence on the renormalisation scale μ_R enters only at NLO QCD accuracy. Therefore, the naive approach of scale variations would in turn lead to artificially small QCD scale uncertainties both at LO and NLO accuracy. This fact is very important also because the NLO EW corrections, the NLO₂, can be potentially larger than the residual scale uncertainties that are obtained via the independent variation of μ_F and μ_R by a factor of two.

A calculation at next-to-next-to-leading-order (NNLO) QCD accuracy would in principle help, but at the moment is unfeasible. Indeed, no NNLO QCD calculation for a 2 \rightarrow 3 process with a massive coloured particle in the final state has ever been performed. In order to amend this situation, we follow the approach of Ref. [11], where the case of tHj production has been considered. This approach relies on the fact that predictions at LO and especially NLO QCD accuracy can be calculated in the 5FS, but also in the 4FS, and the difference between the two predictions at NLO QCD accuracy can be interpreted as an additional estimate of the uncertainty due to missing higher-order terms in α_s . We briefly recall in the following the rationale behind this interpretation.

Given any scale Q involved in the process, besides power corrections of order $(m_b/Q)^n$ with $n > 0$, which can be taken into account only in the 4FS, the two flavour schemes effectively correspond to a rearrangement of logarithms of the form $\alpha_s^n \log^k(Q/m_b)$ with at most $k \leq n$. For $Q \gg m_b$, *i.e.* for instance for total cross sections without hard cuts such as jet vetoes or distributions far from the threshold region, power corrections are negligible and the aforementioned logarithms are large. In the 5FS, these large logarithms are resummed and therefore better estimated. On the other hand, at variance with the 5FS, in the 4FS the μ_R dependence enters already at LO for the processes we are considering and therefore NLO calculations involve a truly NLO dependence on μ_R . Moreover, at the differential level, the presence of an additional particle in the final state resembles a more realistic signature and, *e.g.*, eliminates or at least softens some of the sharp edges or endpoints that are typical of fixed-order calculations, where the recoil momentum of any particle is shared among the few others in the final state. Last but not least, close to the threshold, power corrections are taken into account. See also Refs. [27, 28] for a more detailed and general discussion on the differences between 4FS and 5FS prediction for b -initiated processes.

As already said, in order to achieve a more realistic estimate of the uncertainty due to missing higher-order terms in α_s , we will take into account the flavour-scheme dependence in our theory uncertainty, as done in Ref. [11]. However, we cannot straightforwardly extend this strategy to our calculation. Indeed, at variance with the study presented here, Ref. [11] focussed only on the t -channel mode in tHj production and especially did not take into account NLO EW corrections, the NLO₂ contribution in Eq. (2). Therefore, we need to slightly modify this strategy in order to adapt it to our set-up. In the following, we describe how we calculate and combine theory uncertainties related to the flavour-scheme dependence and scale variations. Afterwards, in the next section, we discuss the problems related to the separation of the different production modes (t -channel, s -channel and W boson associated production) and we motivate on the basis of those problems the rationale behind the strategy that we have adopted.

For any observable, we define as $\text{NLO}_{\text{QCD},t\text{-ch.}}^{4\text{FS}}$ and $\text{NLO}_{\text{QCD},t\text{-ch.}}^{5\text{FS}}$ the prediction at NLO QCD accuracy where only the t -channel diagrams have been taken into account. There is no difference for the tHj , tZj and $t\ell^+\ell^-j$ production, so we do not specify them in the following discussion. With the notation $(\text{NLO}_{\text{QCD},t\text{-ch.}}^{4\text{FS}})_{-\Delta_-^{4\text{FS}}}^{+\Delta_+^{4\text{FS}}}$ and $(\text{NLO}_{\text{QCD},t\text{-ch.}}^{5\text{FS}})_{-\Delta_-^{5\text{FS}}}^{+\Delta_+^{5\text{FS}}}$ we indicate, together with the central value, the *relative* difference with the upper (Δ_+) and lower (Δ_-) values of the scale-uncertainty band, which we evaluate via the 9-point independent variation of the renormalisation and factorisation scale. Similarly, $(\text{NLO}_{\text{QCD+EW}}^{5\text{FS}})_{-\Delta_-^{5\text{FS}}}^{+\Delta_+^{5\text{FS}}}$ denotes with a similar notation the prediction, with scale uncertainties, at NLO QCD+EW accuracy in the

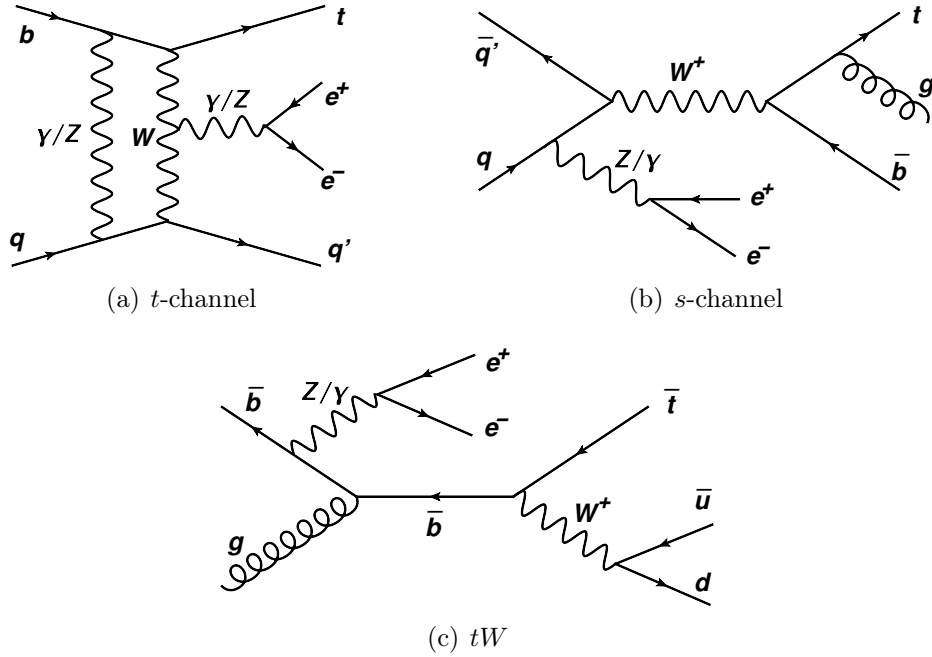


Figure 1: Representative Feynman diagrams for the different channels entering the $\text{NLO}_{\text{QCD+EW}}$ predictions for $t\ell^+\ell^-j$ production. The diagram 1(a) contributes to the NLO_2 , while the diagrams 1(b) and 1(c) contribute to the NLO_1 . Similar diagrams are present for tZj production, while in tHj production the Higgs boson does not couple to the initial-state particles.

5FS, where the tilde on top of Δ has been added just for distinguishing them from the purely QCD case. We notice that $(\text{NLO}_{\text{QCD+EW}}^{5\text{FS}})_{-\tilde{\Delta}_{5\text{FS}}^+}$ is not obtained by selecting t -channel diagrams, but retaining all the possible contributions: not only t -channel, but also s -channel and tW associated production with subsequent W boson hadronic decay, see Fig. 1 for representative diagrams.

In order to combine scale and flavour-scheme uncertainties at NLO QCD accuracy, we consider the t -channel only and we define the quantity $(\text{NLO}_{\text{QCD,t-ch.}}^{5\text{FS}})_{-\tilde{\Delta}_{4-5\text{FS}}^+}$ via the envelope of the two bands given by $(\text{NLO}_{\text{QCD,t-ch.}}^{4\text{FS}})_{-\tilde{\Delta}_{4\text{FS}}^+}$ and $(\text{NLO}_{\text{QCD,t-ch.}}^{5\text{FS}})_{-\tilde{\Delta}_{5\text{FS}}^+}$, where the central value is set equal to the one in the 5FS. The quantities $\tilde{\Delta}_{4-5\text{FS}}^+$ and $\tilde{\Delta}_{4-5\text{FS}}^-$ are then propagated to the $\text{NLO}_{\text{QCD+EW}}$ prediction in the 5FS. In conclusion, in order to combine flavour-scheme and scale uncertainties and take into account EW corrections, not only for t -channel, we will employ as reference prediction the quantity $(\text{NLO}_{\text{QCD+EW}}^{5\text{FS}})_{-\tilde{\Delta}_{4-5\text{FS}}^+}$ and in the case of QCD only corrections, in order to be consistent, we will use the quantity $(\text{NLO}_{\text{QCD}}^{5\text{FS}})_{-\tilde{\Delta}_{4-5\text{FS}}^+}$, where in the quantity $\text{NLO}_{\text{QCD}}^{5\text{FS}}$ the requirement of t -channel only is not applied. In Sec. 3 predictions obtained following this approach will be simply denoted by $5\text{FS}_{4-5}^{\text{scale}}$.

2.2 Separation of different production modes

In this section we explain why we cannot select the t -channel mode and at the same time take into account NLO EW corrections. Moreover, we explain why we believe that not singling out the t -channel mode is anyway preferable for providing reference predictions for experimental measurements. After this explanation, we will motivate the strategy that we have designed in order to take into account flavour-scheme dependence and scale variations in our theory uncertainty.

First of all, it is important to point out that the division of single top production into t -channel, s -channel and tW associated production is conventional and especially it is clearly defined only under certain conditions that depend on the flavour-scheme choice and the perturbative order of the calculation. The presence of a Higgs boson or a Z boson or an $\ell^+\ell^-$ pair is irrelevant for the present discussion and therefore it is understood in the following.

In the 5FS, at LO, the production of a single top quark can be divided into the three categories according to the W boson line in the Feynman diagrams: s -channel propagator, t -channel propagator or final-state associated production. This division is gauge invariant and well defined also at NLO QCD accuracy, however the tW associated production leads to the same final state as $t\bar{t}$ production, which has a much larger cross section, and interferes with it. This occurs when b -quark real emission induces diagrams with an additional top decaying into a Wb pair. At NNLO QCD accuracy, even s - and t -channel topologies start to interfere. When EW corrections are taken into account, the situation becomes more complex. The main reason is that photons in the initial state have to be taken into account. The process $\gamma q \rightarrow t\bar{b}q'$, contributing to the NLO₂ term in Eq. (2), involves t -channel diagrams, s -channel diagrams and the separation is not gauge invariant. Similarly, the process $\gamma b \rightarrow tq\bar{q}'$, contributing also to the NLO₂ term, involves t -channel diagrams and diagrams where a $q\bar{q}'$ pair stems from an s -channel W boson, and also in this case the separation is not gauge invariant. In other words, similarly to the case of tW at NLO QCD, where $t\bar{t}$ diagrams emerge in real-emission corrections, in the NLO EW corrections to tj production in the 5FS we cannot separate in a straightforward and gauge-invariant way the contribution from different production modes. In the 4FS, the situation is even worse. Even with only QCD corrections, the t -channel at NLO can interfere with the s -channel at NNLO and with the W -associated production with $W \rightarrow q\bar{q}'$ decays. Moreover, the tW and $t\bar{t}$ interference is already present at the tree level.

From the previous discussion it is manifest why singling out contributions from t -channel production is very challenging in our calculation. Moreover, we believe that independently of these difficulties, singling out t -channel production should not be done when providing reference values for experimental measurements such as those already performed by the ATLAS and CMS collaboration. Indeed, in these analyses, selection cuts have not been designed to separate the t -channel from the other production modes.

We remind the reader that the origin of this problem is solely due to the fact that we are performing a calculation with unstable particles that are kept stable, and the separation of the different processes is based on intermediate resonances, a procedure not well defined in quantum mechanics due to interference effects. On the contrary, signal regions in experimental analyses are defined via stable particles/objects (jets, b -jets, leptons, *etc.*) emerging from decays. There are two kinds of possible strategies for addressing this problem. First, performing a calculation for the signature itself, as it has been done in Ref. [24] for the NLO QCD+EW corrections in t -channel single-top production or in Refs. [29–31] for NLO QCD corrections in the tW associated production, where in both cases no additional associated Z or H boson production has been taken into account. Second, adopt gauge-violating solutions based on the exclusion of specific diagrams, denoted in the literature as Diagram Removal (DR) [32, 33], or gauge-invariant solutions based on the subtraction of on-shell contributions at the global or local level, denoted in the literature as Diagram Subtraction (DS) [33–35].

The first kind of strategy implies an extremely challenging calculation for the case of single-top production with an extra emission of a Higgs boson, a Z boson or an $\ell^+\ell^-$ pair, especially for the case of EW corrections.² The complexity of such a calculation is well beyond the state-of-the-art predictions available at the moment in the literature. Especially, this level of accuracy is not urgently needed. The second strategy could be in principle used in order to remove the

²This would be equivalent to the calculation of Ref. [24] with at least two additional particles in the final state.

contribution of tW from the NLO corrections, namely, tW production with the subsequent hadronic W boson decay, see Fig. 1(c). However, at variance with the case of the large $t\bar{t}$ contribution emerging in tW at NLO QCD accuracy [32, 36], the tW cross section is in fact smaller than the single-top t -channel cross section. Moreover, signal regions in experimental analyses are not designed in order to suppress the tW contribution. For this reason, we believe that also the second strategy is not improving the theoretical predictions that are relevant for experimental analyses. Therefore, for the processes studied in this work, results obtained with no restrictions on the diagrams and the flavour of the jet in the final state should be preferred. From now on, the tW associated production with the subsequent hadronic W boson decay (see Fig. 1(c)) will be denoted as tW_h .

On the basis of the previous discussion, we now can motivate our strategy for evaluating flavour-scheme uncertainties. In particular, in the following we explain why we consider only differences among t -channel contributions at NLO QCD accuracy for the flavour-scheme uncertainties of $\text{NLO}_{\text{QCD+EW}}$ predictions for which the t -channel selection is not performed.

The main problem is that, without separating the different productions modes, it is not straightforward to compare NLO QCD predictions for tj production in the 4FS and in the 5FS. Indeed, in the 4FS, the t -channel process corresponds to the process $pp \rightarrow tj\bar{b}$, which however includes also real emissions of gluons from s -channel diagrams. Unless a minimum p_T for the light jet is required, these contributions are not infrared (IR) finite and therefore have to be excluded, both at LO and at NLO. On the other hand, the s -channel contribution not only is very small, but it also does not depend on the bottom PDF; its impact on the flavour-scheme choice is completely negligible. Thus, the s -channel contribution can be safely removed in the estimate of the flavour-scheme uncertainties. In principle, one may retain the contribution of tW_h production arising from NLO corrections, however we believe it is preferable to exclude it, too. The reason is that the tW_h contribution is of Born type both in the 4FS and in the 5FS. Therefore, being proportional to α_s^2 in the 4FS and to α_s in the 5FS, in the former case it entails a larger dependence on μ_R . Moreover, in the 4FS also a larger dependence on μ_F is present, since large logarithms involving m_b are not resummed. In other words, concerning the tW_h contribution in our calculation, the 4FS simply leads to a less accurate prediction than the 5FS one. In conclusion, we use the t -channel only contributions for the estimate of flavour-scheme uncertainties. NLO EW corrections are not expected to play a major role in the flavour-scheme uncertainty and, as will also be shown in Sec. 3.1, their impact on the scale uncertainties is below the percent level. Therefore, also for $\text{NLO}_{\text{QCD+EW}}$ predictions, the estimate of flavour-scheme uncertainties is performed via the comparison of NLO_{QCD} t -channel predictions.³ The quantities $(\text{NLO}_{\text{QCD+EW}}^{5\text{FS}})_{-\Delta_{4-5\text{FS}}}^{+\Delta_{4-5\text{FS}}}$ and $(\text{NLO}_{\text{QCD}}^{5\text{FS}})_{-\Delta_{4-5\text{FS}}}^{+\Delta_{4-5\text{FS}}}$ that have been introduced in Sec. 2.1 precisely correspond to the strategy that we have just outlined and, as already said, will be denoted in Sec. 3 as $5\text{FS}_{4-5}^{\text{scale}}$.

From the previous discussion it also becomes clear why the so-called “multiplicative approach” for the combination of NLO QCD and NLO EW corrections is not expected to lead to improved predictions. At variance with the standard additive procedure leading to the $\text{NLO}_{\text{QCD+EW}}$ predictions, which is also denoted in the literature as “additive approach”, in the multiplicative approach the NLO_2 term is not only added on top of the NLO_{QCD} predictions but it is also multiplied by the QCD K -factor, the $(\text{LO}_1 + \text{NLO}_1)/\text{LO}_1$ ratio. The rationale behind this choice is the possibility of estimating mixed QCD–EW NNLO corrections of $\mathcal{O}(\alpha_s\alpha)$ w.r.t. the LO predictions and at the same time reduce the scale dependence of the $\text{NLO}_{\text{QCD+EW}}$ ones. However, the multiplicative approach is justified only when the dominant contributions from both the NLO_1 and NLO_2 terms factorise, the typical case being soft QCD corrections

³Since very recently NLO EW corrections can be calculated also in the 4FS via `MADGRAPH5_AMC@NLO` [37].

from the former and weak Sudakov logarithms from the latter. In our calculation both NLO QCD and NLO EW corrections induce the opening of a new production mechanisms, namely the tW_h associated production. First, the tW_h component in the NLO QCD corrections is not negligible, as also documented in Sec. 3. Second, separating the different production channels is not possible for the case of the EW corrections. For these reasons, in our study we have refrained from combining NLO QCD and NLO EW corrections in the multiplicative approach and we provide predictions only in the additive approach, $\text{NLO}_{\text{QCD+EW}}$.

2.3 Input Parameters

In this paper we provide results for proton–proton collisions at the LHC, with a centre-of-mass energy of 13 TeV. In our calculation we use the following on-shell input parameters

$$\begin{aligned} m_Z &= 91.188 \text{ GeV}, & m_W &= 80.385 \text{ GeV}, & m_H &= 125 \text{ GeV}, \\ \Gamma_Z &= 2.49707 \text{ GeV}, & \Gamma_W &= 2.09026 \text{ GeV}, & \Gamma_H &= 0, \\ m_t &= 173.3 \text{ GeV}, & m_b &= 4.92 \text{ GeV}, & \Gamma_t &= 0, \end{aligned} \quad (3)$$

and employ the complex mass scheme [38, 39]. We have set $\Gamma_H = 0$ and $\Gamma_t = 0$, since in our calculation there is always an external on-shell top quark and in the case of tHj production an external on-shell Higgs boson. We also set $\Gamma_Z = 0$ in the case of tZj production. The value $m_b = 4.92$ GeV directly enters our calculations only in the 4FS. It has been chosen in order to be consistent with the value used in the PDF evolution of the PDF sets that we employ for the calculations in the 5FS. We discuss later in detail the PDF-set choice. We also note that while in the 5FS the Higgs boson does not couple to the b quark, it does in the 4FS. However, the contribution of diagrams involving this coupling is subleading in the case of tHj production, where a top quark is present in the final state and a W -boson in the propagator, leading to much larger Higgs couplings. For this reason, in the 4FS we can safely use the on-shell m_b value also for the bottom Yukawa interaction. See also Ref. [11] for more details.

In our calculation EW interactions are renormalised in the G_μ -scheme with

$$G_\mu = 1.16639 \cdot 10^{-5} \text{ GeV}^{-2}, \quad (4)$$

while QCD interactions are renormalised in the $\overline{\text{MS}}$ -scheme with five active flavour in the 5FS and four active flavour in the 4FS. The numerical input and the μ_R dependence of α_s is directly taken from the PDF sets used in the calculation. In order to estimate QCD scale uncertainties, we vary independently by a factor of two μ_r and μ_f around the central value μ_0 defined as follows,

$$\mu_0 \equiv H_T/6 = \frac{\sum_i m_{T,i}}{6}, \quad i = t, H, b \quad \text{for } tHj, \quad (5)$$

$$\mu_0 \equiv H_T/6 = \frac{\sum_i m_{T,i}}{6}, \quad i = t, Z, b \quad \text{for } tZj, \quad (6)$$

$$\mu_0 \equiv H_T/6 = \frac{\sum_i m_{T,i}}{6}, \quad i = t, Z(\ell^+\ell^-), b \quad \text{for } t\ell^+\ell^-j. \quad (7)$$

The scale definition in Eq. (5) is based on the findings of Refs. [11, 27] and the same rationale has been used for Eqs. (6) and (7). With t and b we refer to both quarks and antiquarks, and the momentum of the bottom (anti)quark is set to zero when this particle is not present in the final state⁴. More details about the scale dependence will be discussed in Sec. 3.1.1.

⁴Since in our calculation there are not $\gamma, g \rightarrow b\bar{b}$ splittings in the final state, this definition is IR safe.

The choice of the PDF set is motivated by a few aspects that are explained in the following. First, our calculation is performed at NLO QCD+EW accuracy and therefore (at least) the same level of accuracy has to be present for the PDFs themselves. Second, in order to evaluate flavour-scheme uncertainties, both a 4FS and a 5FS version of the same PDF fit have to be available. Therefore, the only three possible options at the moment are: NNPDF3.0 [40, 41], NNPDF3.1 [42, 43] and MMHT2014/MMHT2015 [44, 45]. All these three sets are accurate up to NNLO in QCD and NLO in QED accuracy and include a photon density based on the LUXQED parameterisation [46, 47]. The set NNPDF3.1 should be preferred over the NNPDF3.0 one, being an improvement of the former, and we choose it for our calculations. Notably, in the case of b -initiated processes this improvement cannot be neglected. We have verified that results in the 5FS obtained with NNPDF3.1 and NNPDF3.0 at NLO QCD accuracy are not compatible within their PDF uncertainties; the difference between them is several times larger than the respective PDF uncertainties. These differences have to be attributed to the different numerical input values for m_b in the NNPDF3.0 and NNPDF3.1 PDF fits,⁵ which can induce large effects on the bottom PDF and in turn to the bottom–gluon luminosity, entering the LO predictions for all the processes considered in this paper. Especially, in our calculation we set $\mu_0 = H_T/6$, which is quite small, and the smaller the factorisation scale, the larger the effect induced by a different m_b value, since m_b determines the threshold condition for the bottom-quark PDF. On the other hand, this effect is smaller if instead of NLO PDFs one employs PDFs at NNLO accuracy. For this reason we suggest to avoid to use of NLO PDFs for the calculation of the processes considered in this work and we adopt NNLO PDFs. We also note that with this choice NNPDF3.1 and MMHT2014/MMHT2015 predictions are very well compatible. As a last remark we want also point out that, to the best of our knowledge, no 4FS PDF set including a photon PDF and NLO QED effects is available at the moment, but would be necessary for NLO EW corrections in the 4FS.

Finally, we describe the clustering procedure that we perform in order to obtain jets and dressed leptons. First of all we recombine possible photons that are present in the final state, due to NLO EW corrections or shower effects, with leptons. In fact, this step concerns only the $t\ell^+\ell^-j$ process. A dressed lepton is obtained by recombining a bare lepton ℓ with any photon γ satisfying the condition

$$\Delta R(\ell, \gamma) < 0.1, \quad (8)$$

where $\Delta R(\ell, \gamma) \equiv \sqrt{(\Delta\eta(\ell, \gamma))^2 + (\Delta\phi(\ell, \gamma))^2}$ and $\eta(\ell, \gamma)$ and $\Delta\phi(\ell, \gamma)$ are the difference of the bare-lepton and photon pseudorapidities and azimuthal angles, respectively. In case that the condition (8) is satisfied for both ℓ^+ and ℓ^- , the photon is clustered together with the bare lepton for which $\Delta R(\ell, \gamma)$ is the smallest. After this, we cluster jets via the anti- k_T algorithm [49] as implemented in FASTJET [50] using the parameters

$$p_T^{\min} = 25 \text{ GeV}, \quad R = 0.5, \quad (9)$$

and including also the previously unrecombined photons in the clustering procedure. This means that in our calculation, especially at fixed order, a jet can correspond to a single photon.⁶ However, it is important to note that in this work the jet definition is relevant only for differential distributions and not for total cross sections. Indeed, the tHj , tZj and $t\ell^+\ell^-j$ processes are all properly defined and IR finite without tagging any jet. When we will consider b -jets, we will simply refer to jets containing a bottom (anti)quark, without any restriction on their pseudorapidity. Also, since in our calculation there are no $\gamma, g \rightarrow b\bar{b}$ splittings in the final state,

⁵We explicitly verified that these effects originate from the different value of the mass of the bottom quark via the NNPDF2.1 PDF sets [48], which allows to use different values for m_b ; consistent deviations have been found.

⁶In many LHC analyses jets are defined with up to 99% of their energy of electromagnetic origin and even up to 90% that can be associated to a single photon. More details can be found in Ref. [20].

b -jets cannot include more than one bottom (anti)quark and no IR safety problems are present in their definition also in the 5FS.

3 Numerical Results

In this section we present and discuss the numerical results of our study. We start with results concerning total cross sections, Sec. 3.1, and afterwards we comment in detail on the case of differential distributions in Sec. 3.2. In both cases, following the strategy described in Sec. 2.1, we compare 4FS and 5FS results in order to evaluate flavour-scheme and scale uncertainties and then we quantify and discuss the impact of electroweak corrections. For the $t\ell^+\ell^-j$ process we show results for two different selection cuts on the invariant mass of the lepton pair $m(\ell^+\ell^-)$:

1. $m(\ell^+\ell^-) > 30$ GeV, dubbed as “inclusive”,
2. $|m(\ell^+\ell^-) - m_Z| < 10$ GeV, dubbed as Z -peak.

The first choice is inspired by the experimental measurements of Refs. [1, 4], which report unfolded results for this kinematic region. The second choice is motivated by the experimental analysis of Ref. [4], which applies this requirement when selecting the events. Finally, in Sec. 3.3, we discuss the impact of the parton shower, including or not QED effects, on top of NLO QCD predictions for the specific case of $t\ell^+\ell^-j$ production.

All results in this section have been obtained via the MADGRAPH5_AMC@NLO framework [15]. Results including NLO QCD and EW corrections employ the latest version of MADGRAPH5_AMC@NLO [16], which is publicly available and allows to calculate NLO EW corrections, and more in general predictions at complete-NLO accuracy, for any SM process. The MADGRAPH5_AMC@NLO framework [15] deals with IR singularities via the so-called FKS method [51, 52], which has been automated in MADFKS [53, 54]. One-loop amplitudes are evaluated via different types of integral-reduction techniques, namely, the OPP method [55] or the Laurent-series expansion [56], and techniques for tensor-integral reduction [57–59]. The module MADLOOP [60], which is employed for generating the amplitudes, automates these techniques and switches dynamically among them. We remind the reader that the codes CUTTOOLS [61], NINJA [62, 63] and COLLIER [64] are employed within MADLOOP, which also includes an in-house implementation of the OPENLOOPS optimisation [65].

3.1 Inclusive results

3.1.1 QCD scale uncertainties in the 4FS and 5FS

For the determination of scale and flavour-scheme uncertainties we follow the strategy that has been described in Sec. 2.1. Therefore, according to this strategy, in this section we focus on 4FS and 5FS predictions for the t -channel contributions to the tHj , tZj and $t\ell^+\ell^-j$ processes. In analogy with Ref. [11], which focuses on tHj production, we analyse the 4FS and 5FS scale dependence at LO and NLO in QCD for the four processes that we consider. We use the setup described in the previous section and to this purpose we vary the central value μ_0 for the renormalisation and factorisation scale, which has been defined in Eq. (7), up and down by a factor of 8. In particular, in the main panel of each of the plots in Fig. 2, the solid lines correspond to the case $\mu_R = \mu_F = r_\mu\mu_0$, where $1/8 < r_\mu < 8$. At NLO, we also explore the impact of non-equal μ_R and μ_F values (off-diagonal variation). For a given $\mu_R = \mu_F$, the coloured bands in Fig. 2 show the range of cross sections obtained by either keeping μ_R or μ_F fixed at $r_\mu\mu_0$ and moving the other one. In both cases, the variation is performed in the range $1/2 < \mu_F/\mu_R < 2$.⁷ In each of the plots of Fig. 2 we also show the QCD K -factor, namely the

⁷This is equivalent to the 7-point variation around the central value $\mu_R = \mu_F = r_\mu\mu_0$.

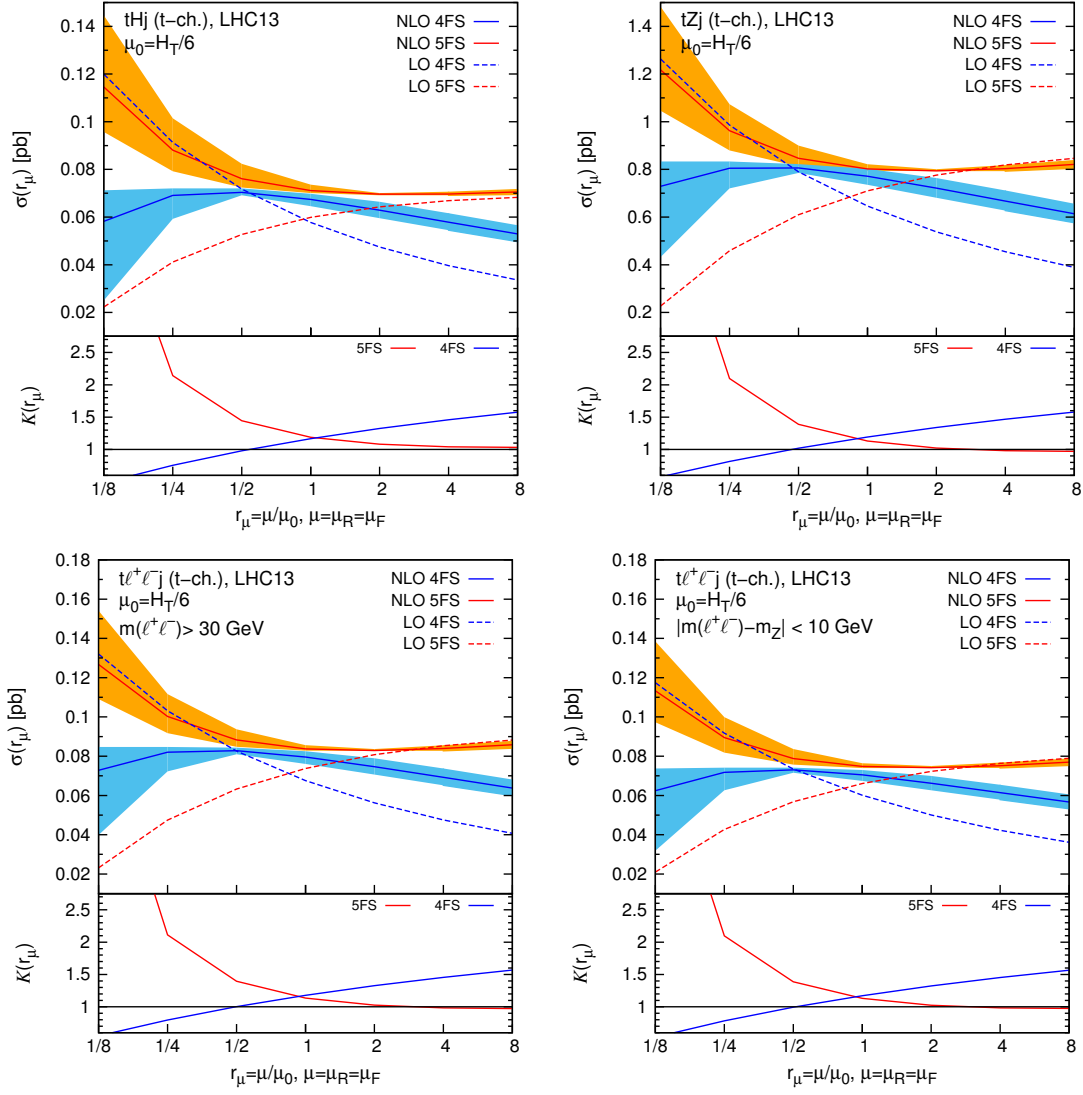


Figure 2: Scale dependence of total cross sections for tHj production (top-left), tZj production (top-right) and $t\ell^+\ell^-j$ production for the “inclusive” (bottom-left) and Z -peak (bottom-right) case in the 4FS and 5FS.

ratio between the NLO_{QCD} and LO predictions, in the lower inset, for both the 4FS and the 5FS.

The first observation is that all four processes behave in a very similar way and the following discussion applies to all of them. NLO QCD corrections reduce the scale uncertainties for both the 4FS and 5FS predictions. The difference between the two schemes is minimised in the region of $\mu_0/2 < \mu < \mu_0$, with the two uncertainty bands touching each other. In this scale region, the difference between the central values lies in the 5% ballpark. The 5FS K -factor strongly increases at low scales and approaches the value of 1 at high scales, whilst in the 4FS QCD corrections decrease the cross section at low scales (K -factor < 1). Given the flatness of the NLO plots shown in Fig. 2 and how narrow the bands of the off-diagonal variation are, it is clear that if we consider only the 4FS or 5FS with the typical scale variation of a factor of two up and down, we will obtain very small uncertainties. These scale uncertainties will not be large enough to enclose both the 4FS and 5FS central values. Therefore, the combination of 4FS and 5FS uncertainties, as described in the previous section, is necessary in order to properly account for missing higher-order QCD effects.

3.1.2 NLO QCD+EW predictions

We proceed to the computation of total cross sections at NLO QCD+EW accuracy, without selecting t -channel diagrams; s -channel and tW_h contributions are retained as explained in Sec. 2.2. Inclusive results for the processes that we consider in this work, tHj , tZj and $t\ell^+\ell^-j$, are shown in Tab. 1, using the settings described in Sec. 2. The two dilepton invariant mass cuts for $t\ell^+\ell^-j$ will allow us to investigate the impact of EW corrections and compare this to the result for the undecayed tZj process.

Accuracy	Channel	FS	tHj	tZj
NLO _{QCD}	t -ch.	4FS	68.1(1) ^{+2.7(+4.0%)} _{-4.5(-6.6%)} ^{+0.4(+0.5%)} _{-0.4(-0.5%)}	764(1) ^{+33(+4.3%)} _{-48(-6.2%)} ^{+3(+0.4%)} _{-3(-0.4%)}
		5FS	71.3(1) ^{+5.2(+7.2%)} _{-1.7(-2.4%)} ^{+0.3(+0.5%)} _{-0.3(-0.5%)}	805(1) ^{+45(+5.5%)} _{-8(-1.0%)} ^{+3(+0.4%)} _{-3(-0.4%)}
		5FS ₄₋₅ ^{scale}	71.3(1) ^{+5.2(+7.2%)} _{-7.7(-10.9%)} ^{+0.3(+0.5%)} _{-0.3(-0.5%)}	805(1) ^{+45(+5.5%)} _{-89(-11.1%)} ^{+3(+0.4%)} _{-3(-0.4%)}
NLO _{QCD}	t -ch., s -ch., tW_h	5FS	85.1(2) ^{+5.4(+6.4%)} _{-2.3(-2.7%)} ^{+0.5(+0.6%)} _{-0.5(-0.6%)}	895(2) ^{+46(+5.1%)} _{-16(-1.8%)} ^{+4(+0.4%)} _{-4(-0.4%)}
		5FS ₄₋₅ ^{scale}	85.1(2) ^{+6.2(+7.2%)} _{-9.2(-10.9%)} ^{+0.5(+0.6%)} _{-0.5(-0.6%)}	895(2) ^{+50(+5.5%)} _{-99(-11.1%)} ^{+4(+0.4%)} _{-4(-0.4%)}
NLO _{QCD+EW}	t -ch., s -ch., tW_h	5FS	82.2(2) ^{+5.6(+6.8%)} _{-2.4(-2.9%)} ^{+0.5(+0.6%)} _{-0.5(-0.6%)}	904(2) ^{+42(+4.7%)} _{-19(-2.1%)} ^{+4(+0.4%)} _{-4(-0.4%)}
		5FS ₄₋₅ ^{scale}	82.2(2) ^{+5.9(+7.2%)} _{-8.9(-10.9%)} ^{+0.5(+0.6%)} _{-0.5(-0.6%)}	904(2) ^{+50(+5.5%)} _{-100(-11.1%)} ^{+4(+0.4%)} _{-4(-0.4%)}
Accuracy	Channel	FS	$t\ell^+\ell^-j$ (“inclusive”)	$t\ell^+\ell^-j$ (Z-peak)
NLO _{QCD}	t -ch.	4FS	80.2(2) ^{+3.7(+4.6%)} _{-5.0(-6.2%)} ^{+0.3(+0.4%)} _{-0.3(-0.4%)}	70.9(2) ^{+3.1(+4.3%)} _{-4.4(-6.2%)} ^{+0.3(+0.4%)} _{-0.3(-0.4%)}
		5FS	84.0(1) ^{+4.7(+5.6%)} _{-0.9(-1.0%)} ^{+0.3(+0.4%)} _{-0.3(-0.4%)}	75.0(1) ^{+4.2(+5.6%)} _{-0.8(-1.0%)} ^{+0.3(+0.4%)} _{-0.3(-0.4%)}
		5FS ₄₋₅ ^{scale}	84.0(1) ^{+4.7(+5.6%)} _{-8.7(-10.4%)} ^{+0.3(+0.4%)} _{-0.3(-0.4%)}	75.0(1) ^{+4.2(+5.6%)} _{-8.5(-11.3%)} ^{+0.3(+0.4%)} _{-0.3(-0.4%)}
NLO _{QCD}	t -ch., s -ch., tW_h	5FS	93.7(2) ^{+4.9(+5.2%)} _{-1.7(-1.8%)} ^{+0.4(+0.4%)} _{-0.4(-0.4%)}	83.4(2) ^{+4.3(+5.1%)} _{-1.5(-1.8%)} ^{+0.4(+0.4%)} _{-0.4(-0.4%)}
		5FS ₄₋₅ ^{scale}	93.7(2) ^{+5.2(+5.6%)} _{-9.7(-10.4%)} ^{+0.4(+0.4%)} _{-0.4(-0.4%)}	83.4(2) ^{+4.6(+5.6%)} _{-9.4(-11.3%)} ^{+0.4(+0.4%)} _{-0.4(-0.4%)}
NLO _{QCD+EW}	t -ch., s -ch., tW_h	5FS	89.6(2) ^{+5.1(+5.7%)} _{-1.7(-1.9%)} ^{+0.4(+0.4%)} _{-0.4(-0.4%)}	77.2(2) ^{+4.9(+6.3%)} _{-1.5(-1.9%)} ^{+0.3(+0.4%)} _{-0.3(-0.4%)}
		5FS ₄₋₅ ^{scale}	89.6(2) ^{+5.0(+5.6%)} _{-9.3(-10.4%)} ^{+0.4(+0.4%)} _{-0.4(-0.4%)}	77.2(2) ^{+4.3(+5.6%)} _{-8.7(-11.3%)} ^{+0.3(+0.4%)} _{-0.3(-0.4%)}

Table 1: Total cross-section for tHj , tZj and $t\ell^+\ell^-j$ production. The uncertainties are scale and PDF of the form \pm absolute (\pm relative in %). The first number in parentheses after the central value is the absolute statistical error.

For each process, in the first block we show results for the t -channel mode in the 4FS and 5FS at NLO in QCD. The 4FS and 5FS combined results, denoted as 5FS₄₋₅^{scale}, are obtained from the combination of the 4FS and 5FS uncertainties as described in detail in Sec. 2.1. In the second block we show the NLO_{QCD} and NLO_{QCD+EW} results in the 5FS including all the contributions (t -ch., s -ch., and tW_h -assoc.). In both cases we show first the pure 5FS result and then the 5FS₄₋₅^{scale} result. The latter is obtained using the 5FS central value, but now assigning as scale uncertainty the rescaled scale-uncertainty from the NLO QCD combination between 4FS and 5FS in the t -channel only case, the result in the third line of the first block. The NLO_{QCD+EW} prediction in the 5FS₄₋₅^{scale} is at the moment the most precise and accurate prediction and should

be taken as reference value for tHj , tZj and $t\ell^+\ell^-j$ production. For a detailed discussion of the motivations and the procedure for assigning the scale and flavour-scheme uncertainties, see Secs. 2.1 and 2.2. Concerning the PDF uncertainties, they are also reported in Tab. 1 and always refer to the central value.

QCD and EW K -factors are reported in Tab. 2, both for the t -channel only case and including all the contributions. Specifically, we show the $\text{NLO}_{\text{QCD}}/\text{LO}$ and the $\text{NLO}_{\text{QCD+EW}}/\text{NLO}_{\text{QCD}}$ ratios, the former both in the 4FS and 5FS, the latter only in the 5FS. Several observations

FS	Channel	K -factor	tHj	tZj
4FS	t -ch.	$\text{NLO}_{\text{QCD}}/\text{LO}$	1.17	1.18
5FS			1.20	1.13
5FS	t -ch.,	$\text{NLO}_{\text{QCD}}/\text{LO}$	1.37	1.24
	s -ch., tW_h	$\text{NLO}_{\text{QCD+EW}}/\text{NLO}_{\text{QCD}}$	0.97	1.01
FS	Channel	K -factor	$t\ell^+\ell^-j$ (“inclusive”)	$t\ell^+\ell^-j$ (Z -peak)
4FS	t -ch.	$\text{NLO}_{\text{QCD}}/\text{LO}$	1.18	1.18
5FS			1.13	1.13
5FS	t -ch.,	$\text{NLO}_{\text{QCD}}/\text{LO}$	1.24	1.24
	s -ch., tW_h	$\text{NLO}_{\text{QCD+EW}}/\text{NLO}_{\text{QCD}}$	0.96	0.93

Table 2: QCD and EW K -factors for all processes. The statistical error is beyond the digits displayed here.

are in order. As already discussed, scale uncertainties of the NLO_{QCD} results are quite small, reaching at most 7%, for the individual 4FS and 5FS predictions for all four processes considered here. At the same time PDF uncertainties remain below the percent level. On the other hand, the t -channel results differ by about 4% between the 4FS and 5FS. Combining the 4FS and 5FS scale variations enlarges the scale uncertainty to at most 11% in the lower direction, in order to encompass the lower edge of the 4FS uncertainty band. Including the s -channel and W -associated channel increases the cross section by 12% for tZj and $t\ell^+\ell^-j$ and 19% for tHj . We notice that NLO QCD scale uncertainties for the pure 5FS results are at the same level with and without the selection of the t -channel modes. This fact supports our strategy for the evaluation of flavour-scheme and scale uncertainties.

Electroweak corrections have a different impact on the four processes considered. They decrease the NLO_{QCD} tHj cross section by 3%, increase the tZj one by 1% whilst the Z -peak results and “inclusive” results are reduced by 7% and 4% respectively. The presence of the $Z \rightarrow \ell^+\ell^-$ decay has a non-negligible impact on the relative size of EW corrections. Indeed, the radiation of photons from the leptons induces the migration of events outside the region $m(\ell^+\ell^-) \sim m_Z$. This is the reason why in the Z -peak case NLO EW corrections are larger in magnitude than in the “inclusive” case: more events migrate outside the selected phase-space region. Nevertheless, for all the processes and cuts considered, the size of EW

corrections is smaller than the combined $5\text{FS}_{4-5}^{\text{scale}}$ scale uncertainty band. Scale uncertainties of the $\text{NLO}_{\text{QCD}+\text{EW}}$ predictions are as expected similar to the NLO_{QCD} ones. We want to point out that, with the exception of the tZj case, if we did not combine 4FS and 5FS scale uncertainties, the $\text{NLO}_{\text{QCD}+\text{EW}}$ central values would have been outside the NLO_{QCD} scale-uncertainty band.

Comparing the tZj and $t\ell^+\ell^-j$ results, we notice that both the Z -peak and “inclusive” results differ from what one would naively expect from the narrow-width approximation $\sigma(t\ell^+\ell^-j) = \sigma(tZj) \times \text{Br}(Z \rightarrow \ell^+\ell^-)$ as there is a significant contribution from off-shell effects and the photon contribution. It is also worth mentioning that moving away from the Z -peak and allowing a looser selection on the lepton pair invariant mass, as done for the “inclusive” case, the cross section increases by more than 15%.

3.2 Differential results

3.2.1 QCD scale uncertainties in the 4FS and 5FS

In order to quantify the differences between the 4FS and 5FS at a differential level we consider several key observables. As a detailed comparison of 4FS and 5FS predictions for tHj production has already been performed in Ref. [11], here our main focus is on tZj and $t\ell^+\ell^-j$ production, but one should note that the same qualitative behaviour is observed for both tHj and tZj production. Moreover, since the impact of NLO QCD corrections is almost identical for tZj and $t\ell^+\ell^-j$ production, in the context of 4FS and 5FS comparisons at the differential level we explicitly consider only tZj production. Again, following the strategy already employed for total rates and explained in Secs. 2.1 and 2.2, in this context we consider t -channel only predictions. We recall that the scale-uncertainty bands for the $5\text{FS}_{4-5}^{\text{scale}}$ predictions, which will be discussed in the next section, correspond to the bin-by-bin envelope of precisely the 4FS and 5FS scale uncertainty bands that we are going to show in this section.

In Fig. 3 we show NLO_{QCD} results for the transverse momentum (p_T) and rapidity or pseudorapidity (y or η) of the hardest light jet ($j_{l,1}$), the hardest b -jet ($j_{b,1}$), top quark and Z boson. In each plot, we show 5FS and 4FS predictions in the main panel. In the first inset we show scale and PDF uncertainties in the 5FS, summed in quadrature and normalised to the corresponding central value. Instead, in the second inset, we show scale uncertainties in the 4FS, again normalised to the corresponding central value, together with the ratio of the 5FS and 4FS predictions.

The largest difference between the 4FS and 5FS is observed for the b -jet pseudo-rapidity distribution, reaching up to 35% in the high rapidity region, which is however beyond the reach of realistic experimental range for b -jet tagging in ATLAS and CMS. This effect is due to the fact that the b -jet is more central in the 5FS computation, as expected and also observed in single top production [66]. It is actually remarkable, how the NLO_{QCD} predictions in the 4FS, which involves a b -jet already at LO, and in the 5FS, which involves a b -jet only at NLO_{QCD} for this process, are close in value.⁸ The hardest light jet is more peripheral and the Z boson more central in the 5FS, but the differences with the corresponding 4FS predictions never exceed 10%. Looking at the transverse momentum distributions we find no striking differences in the shapes for the 4FS and 5FS. Scale uncertainties are similar in size for the top, light jet and Z -boson observables when comparing 4FS and 5FS. For the b -jet however the scale uncertainties are significantly smaller for the 4FS as a b -quark is present already at LO and therefore b -jet observables are computed at NLO QCD accuracy. In the 5FS b -quarks emerge only at NLO and therefore b -jet observables are effectively described at LO accuracy.

⁸We have investigated this aspect and found that NLO QCD corrections are small in the 4FS. Thus, this comparison can also be viewed as NLO QCD in the 5FS versus LO in the 4FS, for which a similar $p_T(j_{b,1})$ spectrum is expected, especially when $|\eta(j_{b,1})|$ is not large.

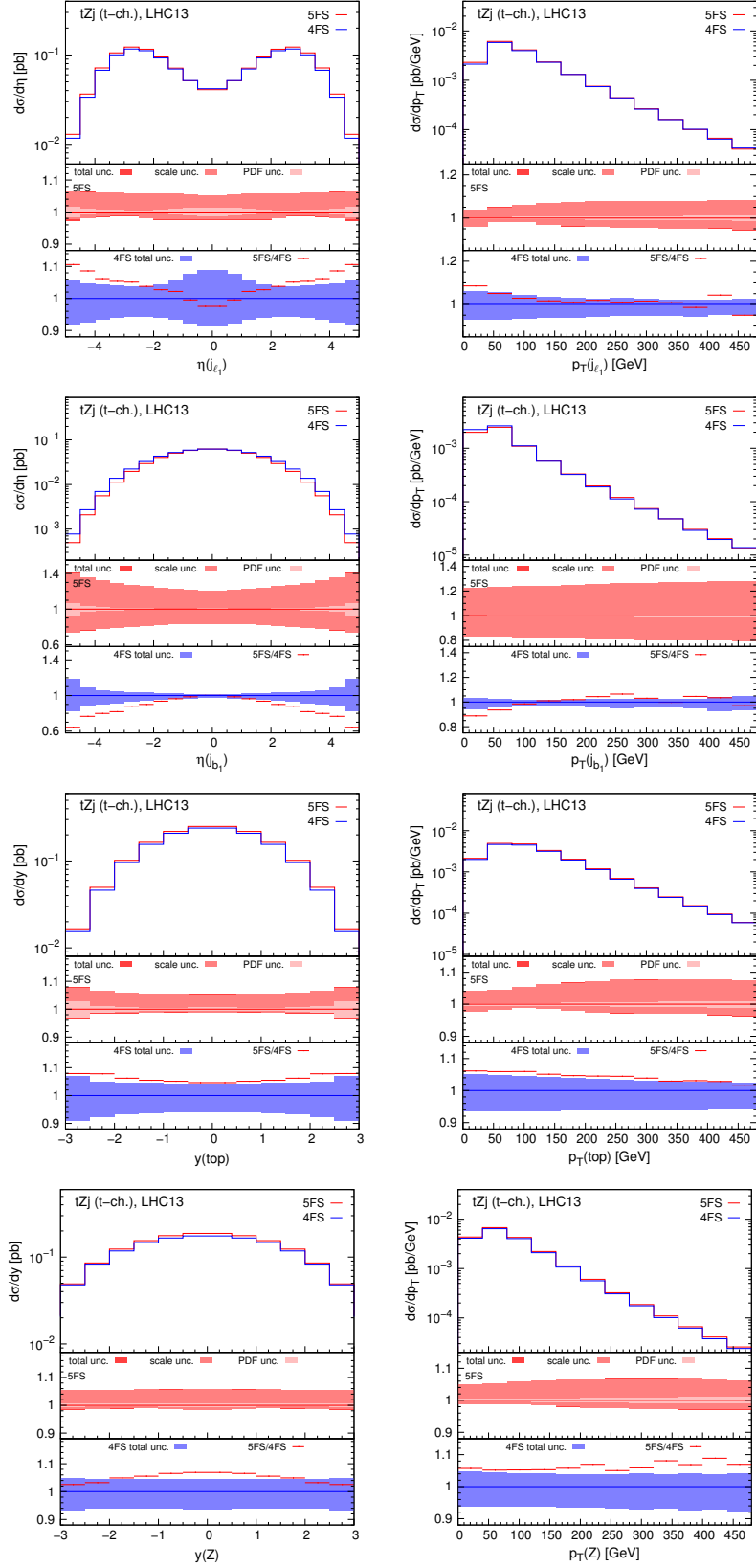


Figure 3: Comparison between 4FS and 5FS for t -channel tZj at NLO QCD. Rapidity and transverse momentum distributions are shown for the hardest light jet, the hardest b -tagged jet, the top quark and the Z boson.

We note here that whilst the qualitative behaviour of tHj and tZj is similar, the differences listed above between 4FS and 5FS are more pronounced for tHj . In particular, the b -jet

transverse-momentum distribution is significantly harder for the 5FS. The presence of differences between the same differential distribution for these two processes is not surprising, since although tHj and tZj are similar processes, they receive different contributions. For instance, the Z boson couples to all particles involved in tZj production, and therefore can be emitted from either the initial or final state or the W propagator whilst the Higgs boson only couples to the top quark and W boson, so it cannot be emitted from the initial state.⁹ This leads to different kinematics and enhances the differences between the two schemes.

3.2.2 NLO QCD+EW predictions

In this section we study differential distributions and explore the impact of EW corrections at the differential level. No t -channel selection is applied and therefore all the t -, s - and tW_h -channel contributions are taken into account. Each one of the Figs. 4–7 have the same layout, which we describe in the following. In each figure we display four different plots for the following distributions: the pseudorapidity and the transverse momentum of the hardest light-jet, the transverse momentum of the top and of the Higgs/ Z boson or $\ell^+\ell^-$ pair. In each plot we show in the main panel the predictions at different accuracies: LO, NLO_{QCD} and NLO_{QCD+EW}, which is our best prediction. In the first inset we show the theory uncertainty band for the NLO_{QCD+EW} prediction, normalised to its central value. The band is given by the sum in quadrature of scale and PDF uncertainties. We remind the reader that we combine 4FS and 5FS scale uncertainties into the 5FS₄₋₅^{scale} one, which has already been described in Sec. 3.1 and in more detail in Secs. 2.1 and 2.2. In the second inset we show the scale uncertainty band for the NLO_{QCD} prediction normalised to its central value. The scale uncertainty band is shown both for the 5FS₄₋₅^{scale}, which is by definition equal to the one of the NLO_{QCD+EW} prediction, and for the 5FS. Also, we show the NLO_{QCD+EW}/NLO_{QCD} ratio for the central values. One can judge the impact of NLO EW corrections by comparing this ratio with the scale uncertainty in the 5FS₄₋₅^{scale}, and also appreciate the difference with the pure 5FS uncertainty.

We start by commenting on Fig. 4, where we show the distributions for the tHj process. We have focussed on the observables for which EW corrections are neither negligible, nor flat. For instance, the shapes of the rapidity of the top quark and Higgs boson are not modified by the NLO EW corrections, with the NLO_{QCD+EW}/NLO_{QCD} ratio being flat over all rapidities and equal to the one already shown in Tab. 2. Similarly, EW corrections to the b -jet distributions are negligible. NLO EW corrections in general reduce the tHj cross section, in particular in the tails of the transverse momentum distributions. This is the typical behaviour of EW corrections. Only in the central region of the $\eta(j_{l,1})$ distribution we observe a positive effect induced by NLO EW corrections. The same effect has been observed for single top production in Ref. [24] and found to be related to the tW_h channel contribution, which enters only at NLO_{QCD} accuracy and populates the central region of the $\eta(j_{l,1})$ distributions. Indeed, when a light jet emerges from the W -boson decay, no enhancement is present in the region close to the beam-pipe axis, at variance with the light jet emerging from t -channel production. This effect can be clearly seen by comparing the LO and NLO_{QCD} lines in the main panel. For more details on this effect see Appendix A in Ref. [24].

For all distributions, the impact of NLO EW corrections remains within the scale uncertainty band of the NLO_{QCD} results, approaching the lower edge of the band in the tails of the distributions. However, this is true only because we employed the 5FS₄₋₅^{scale}. If we had considered only the 5FS scale uncertainties, this would not be the case; NLO EW corrections would shift the central value of the prediction to the lower edge of the NLO_{QCD} scale uncertainty band, and outside of it for the $p_T(j_{l,1})$ and $p_T(H)$ distributions.

⁹As already mentioned, even in the 4FS where $m_b \neq 0$ the emission of a Higgs boson from the bottom-quark fermion line is negligible for this process.

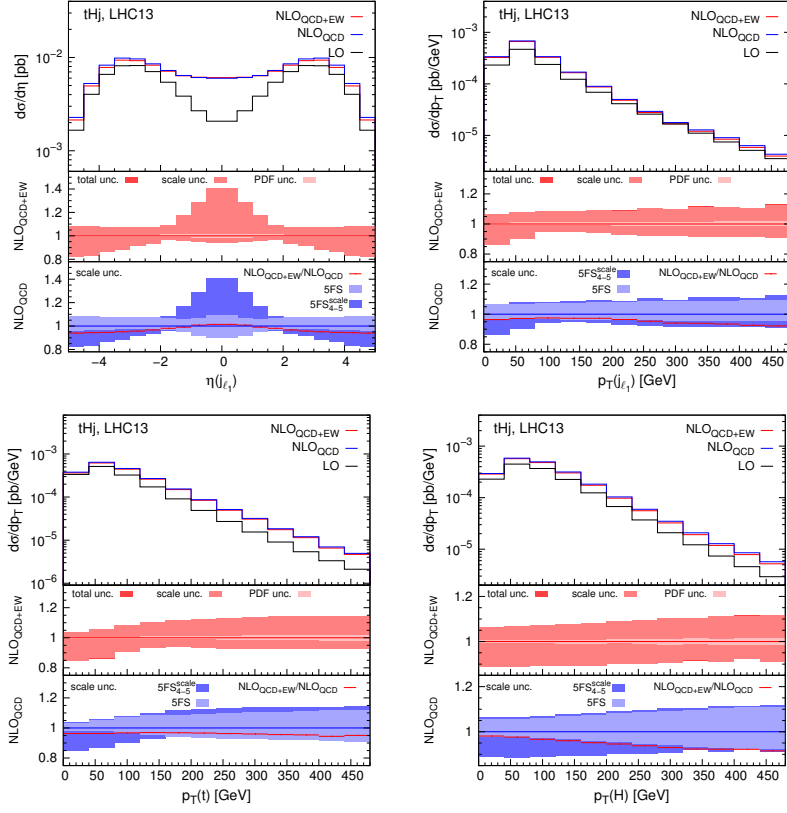


Figure 4: NLO_{QCD+EW} predictions for tHj . In each plot the first inset shows the total uncertainty (flavour-scheme, scale and PDFs) and the second inset shows the NLO_{QCD+EW}/NLO_{QCD} ratio along with the NLO_{QCD} scale uncertainties both in the $5FS_{4-5}^{scale}$ and $5FS$.

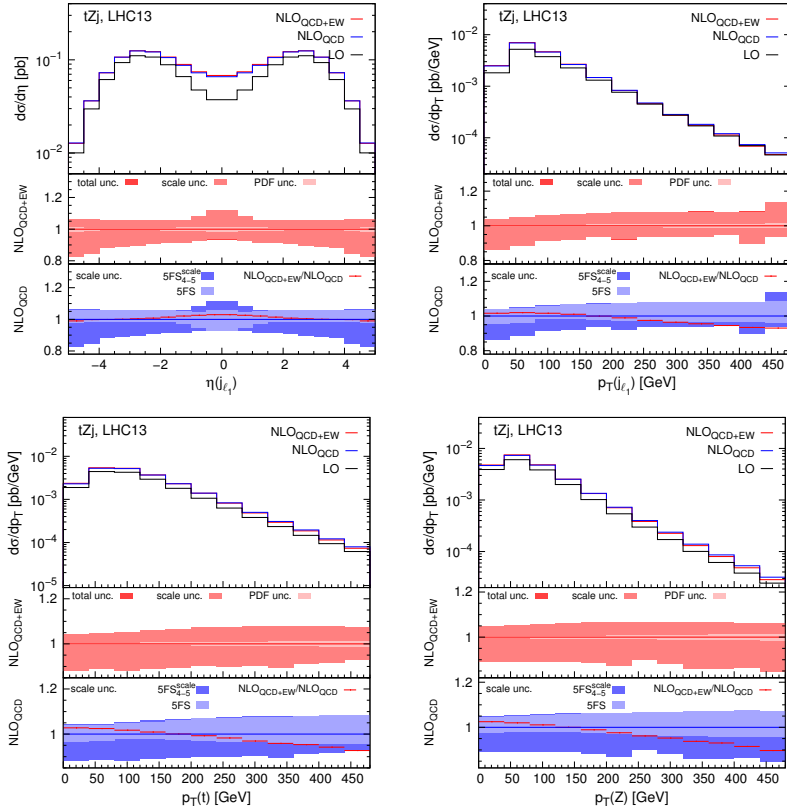


Figure 5: NLO_{QCD+EW} predictions for tZj . The layout of the plots is the same of Fig. 4.

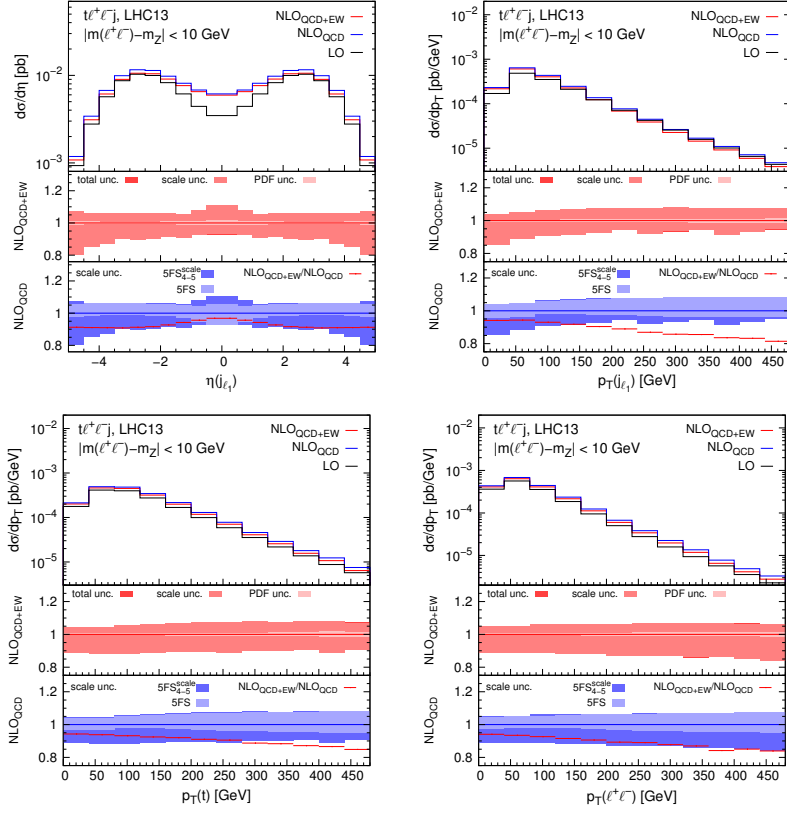


Figure 6: NLO_{QCD+EW} predictions for $t\ell^+\ell^-j$ (Z -peak). The layout of the plots is the same of Fig. 4.

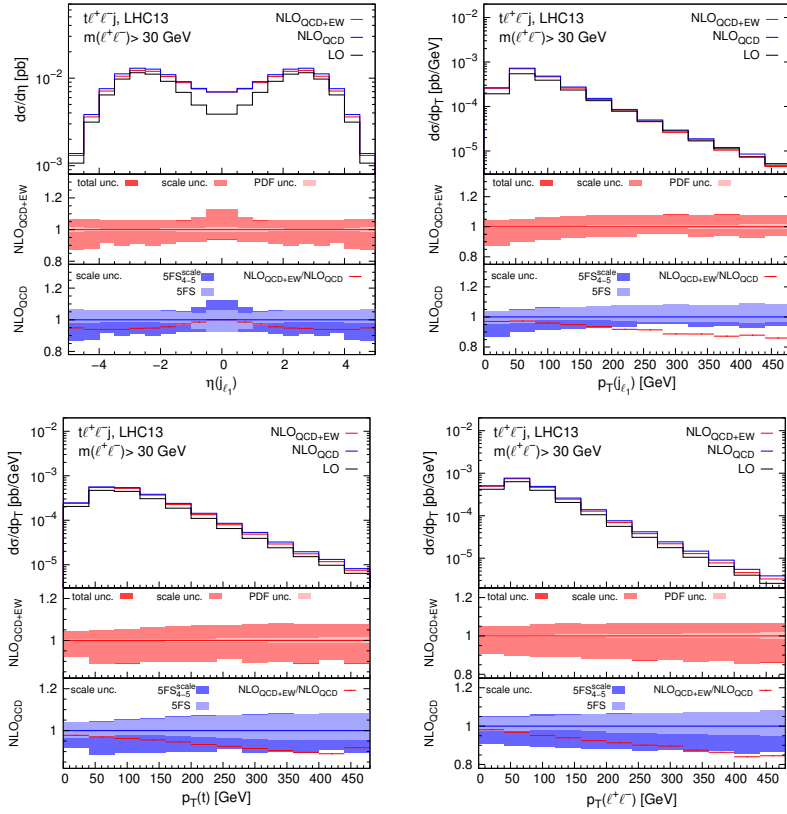


Figure 7: NLO_{QCD+EW} predictions for $t\ell^+\ell^-j$ (“inclusive”). The layout of the plots is the same of Fig. 4.

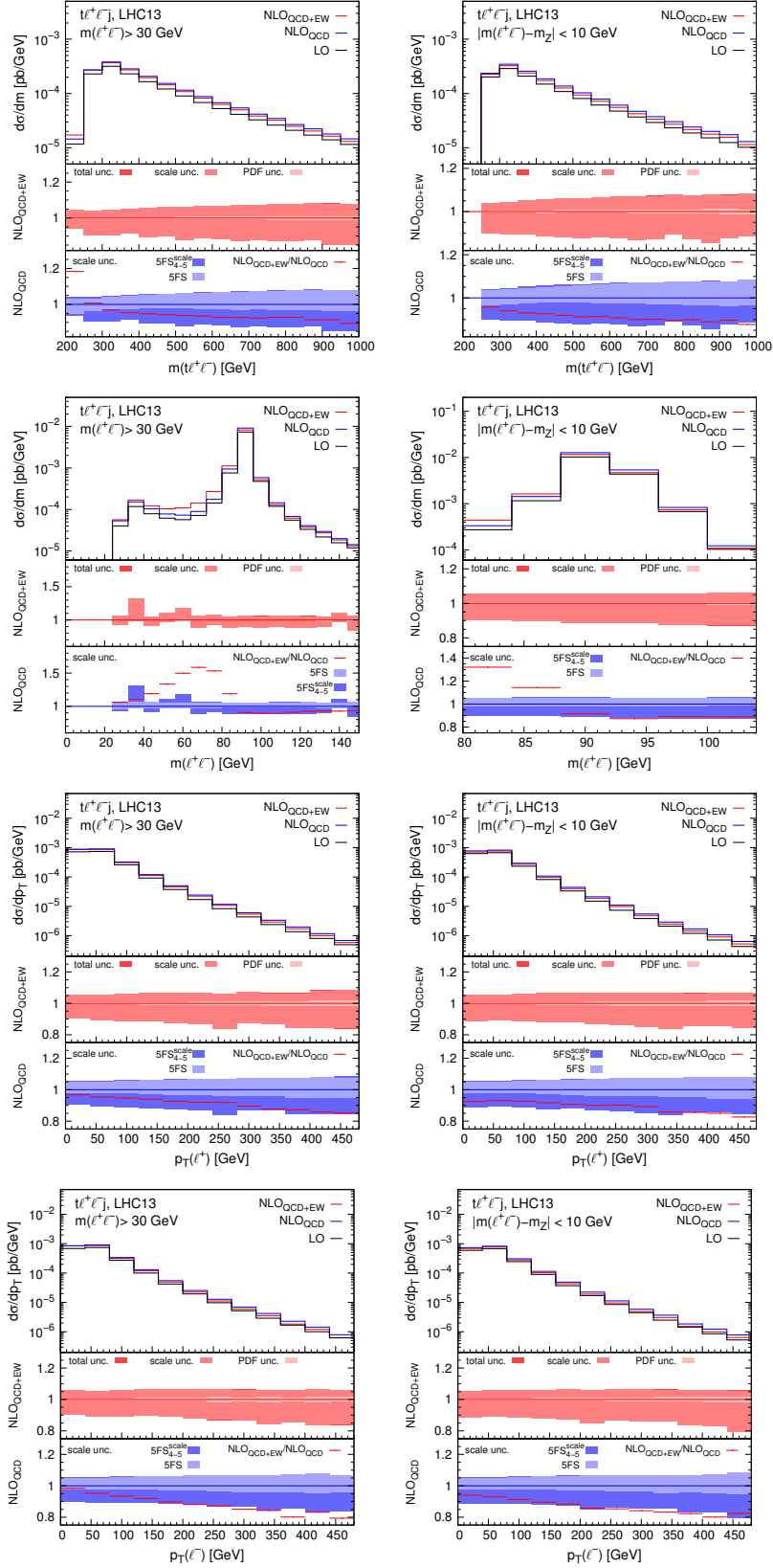


Figure 8: Further plots as in Figs. 6 and 7 for $t\ell^+\ell^-j$ lepton-based observables. The “inclusive” case is displayed on the left while the Z -peak one on the right.

The corresponding results for tZj production are shown in Fig. 5. NLO EW corrections in tZj show the same qualitative features as in tHj with the corrections reaching $\sim 10\%$ in the tail. At low transverse momentum they in fact increase the cross section by a couple of percent.

The corresponding results for $t\ell^+\ell^-j$ production are shown in Figs. 6 and 7 for the Z -peak and “inclusive” selection cuts. Whilst the qualitative behaviour of the NLO EW corrections remains the same as for tZj production, the size of the corrections is larger, reaching up to 15% in the tails of the distributions. Especially, in contrast with tZj and tHj production, the NLO EW corrections are large enough to possibly lie outside the NLO_{QCD} scale-uncertainty band also in the $5\text{FS}_{4-5}^{\text{scale}}$. This happens above 150 GeV in the transverse momentum distribution of the light jet and in the last few bins of the top-quark and dilepton transverse momentum distributions. We notice that in the tails NLO EW corrections are similar in size for Z -peak and “inclusive” selection cuts, while in the rest of the spectrum they are larger in the latter, consistently with the results in Tab. 2. In fact, in the pure 5FS, for the Z -peak selection cuts NLO EW corrections would be outside the scale uncertainty band over the full spectrum, with the exception of central region of the $\eta(j_{i,1})$ distribution.

Finally in the cases of $t\ell^+\ell^-j$, both Z -peak and “inclusive”, we show additional distributions involving the leptons. In Fig. 8 we show the invariant mass of the $t\ell^+\ell^-$ system, the invariant mass of the lepton pair and the transverse momentum distributions of the two leptons. The $t\ell^+\ell^-$ system invariant mass behaves in a similar way for both the “inclusive” and Z -peak results, reaching 10% reduction in the rate in the tail of the distribution. NLO EW corrections have a large impact on the shape of the dilepton invariant mass distribution. Whilst close to the Z -peak, where the bulk of the cross section originates, corrections are negative and relatively small, at lower invariant masses they become very large. Indeed, we see a pronounced bump in the $\text{NLO}_{\text{QCD}+\text{EW}}/\text{NLO}_{\text{QCD}}$ ratio below the Z mass. This is related to the photon emission from the leptons, which reduces the lepton invariant mass due to events migrating to bins with a smaller invariant mass. The NLO EW corrections increase the rate in the region of $50 \text{ GeV} < m(\ell^+\ell^-) < 80 \text{ GeV}$ by up to 60% compared to the NLO_{QCD} result. The same pattern, although smaller in size, is observed even in the Z -peak range, with the impact of NLO EW corrections reaching 30% at the lower end of the distribution. In both cases, the impact of NLO EW corrections is much larger than the NLO_{QCD} scale-uncertainty band, even in the $5\text{FS}_{4-5}^{\text{scale}}$. Finally, we comment on the lepton p_T distributions. These exhibit the typical behaviour of EW corrections, with large (reaching 20%) negative corrections in the tails of the distributions. Using the $5\text{FS}_{4-5}^{\text{scale}}$, the NLO EW corrections lie at the lower edge of the QCD scale-uncertainty bands. In the case of a pure 5FS, they would be outside, both in the Z -peak and “inclusive” case.

3.3 QCD and QED shower effects

In Sec. 3.2 we have computed the NLO EW corrections for various observables and we have found a significant impact in two cases: on the tails of the p_T distributions and especially in the dilepton invariant mass distribution in $t\ell^+\ell^-j$ production. While the former case is due to purely weak effects, namely Sudakov logarithms, the latter originates from QED final-state radiation (FSR). In this section we therefore explore the dependence of QED FSR effects on the recombination parameters for leptons and photons. Also, we investigate the impact of the multiple emission of photons via a shower simulation that includes QED effects.

To this purpose, we generalise (8) into

$$\Delta R(\ell, \gamma) < R_{\text{rec}}^\ell, \quad (10)$$

and we look at the dependence of cross-section predictions on the recombination parameter R_{rec}^ℓ . In the previous sections R_{rec}^ℓ was set equal to 0.1. In principle, if no selection cuts were applied on the leptons, the *inclusive* results would not depend on the value R_{rec}^ℓ . However, when we study the $t\ell^+\ell^-j$ process, in both the “inclusive” and the Z -peak cases, there is an $m(\ell^+\ell^-)$ cut applied. Therefore we expect that not only differential distributions but also total rates

$t\ell^+\ell^-j$ [fb]

Order	settings	“inclusive”	Z-peak
NLO _{QCD+EW}	FO, $R_{\text{rec}}^\ell = 0.1$	89.6(2) ^{+5.1(+5.7%)} _{-1.7(-1.9%)} +0.4(+0.4%) _{-0.4(-0.4%)}	77.2(2) ^{+4.9(+6.3%)} _{-1.5(-1.9%)} +0.3(+0.4%) _{-0.3(-0.4%)}
	FO, $R_{\text{rec}}^\ell = 0.5$	89.5(2) ^{+5.1(+5.7%)} _{-1.7(-1.9%)} +0.4(+0.4%) _{-0.4(-0.4%)}	78.1(2) ^{+4.8(+6.1%)} _{-1.5(-1.9%)} +0.3(+0.4%) _{-0.3(-0.4%)}
NLO _{QCD}	FO	93.7(2) ^{+4.9(+5.2%)} _{-1.7(-1.8%)} +0.4(+0.4%) _{-0.4(-0.4%)}	83.4(2) ^{+4.3(+5.1%)} _{-1.5(-1.8%)} +0.4(+0.4%) _{-0.4(-0.4%)}
	PS _{QCD}	94.0(2) ^{+4.8(+5.1%)} _{-1.7(-1.8%)} +0.4(+0.4%) _{-0.4(-0.4%)}	83.7(2) ^{+4.3(+5.1%)} _{-1.5(-1.8%)} +0.4(+0.4%) _{-0.4(-0.4%)}
	PS _{QCD+QED} , $R_{\text{rec}}^\ell = 0.1$	93.8(2) ^{+4.8(+5.1%)} _{-1.7(-1.8%)} +0.4(+0.4%) _{-0.4(-0.4%)}	81.2(2) ^{+4.1(+5.1%)} _{-1.5(-1.8%)} +0.4(+0.4%) _{-0.4(-0.4%)}
	PS _{QCD+QED} , $R_{\text{rec}}^\ell = 0.5$	93.9(2) ^{+4.8(+5.1%)} _{-1.7(-1.8%)} +0.4(+0.4%) _{-0.4(-0.4%)}	82.3(2) ^{+4.2(+5.1%)} _{-1.5(-1.8%)} +0.4(+0.4%) _{-0.4(-0.4%)}

Table 3: Cross section comparisons for $t\ell^+\ell^-j$.

do depend on R_{rec}^ℓ . For this reason, we consider both the $R_{\text{rec}}^\ell = 0.1$ and $R_{\text{rec}}^\ell = 0.5$ options and we determine the impact on the total rates and the lepton-related distributions. At the same time, we examine whether NLO EW corrections, when they are dominated by QED FSR, can be equivalently simulated by allowing photon emissions within the QCD shower. For this approach we focus on the NLO_{QCD} result and we use the default tune of PYTHIA8 [67, 68] for the parton shower. In order to compare these results with the fixed-order ones, we keep the (anti)top quark stable and we switch on the photon emissions from quarks and leptons. Within the analysis, we apply the same lepton-photon recombination ($R_{\text{rec}}^\ell = 0.1, 0.5$) and the same jet algorithm as at fixed order.

In Tab. 3 we show the cross sections for $t\ell^+\ell^-j$ production. Fixed-order (FO) NLO_{QCD+EW} results are shown for $R_{\text{rec}}^\ell = 0.1$ (the same number of Tab. 1) and $R_{\text{rec}}^\ell = 0.5$ and they are compared to the NLO_{QCD} results, which are shown for different set-ups: fixed-order (FO), matched to the QCD parton shower (PS_{QCD}) via the MC@NLO method [69] and including also QED effects in the shower (PS_{QCD+QED}). In the last case, results are again shown for $R_{\text{rec}}^\ell = 0.1, 0.5$. All the scale uncertainties are in the standard 5FS.

Concerning the FO results at NLO_{QCD+EW} accuracy, for the “inclusive” result there is no visible difference by varying the R_{rec}^ℓ , whereas for the Z-peak one the cross section is slightly increased with $R_{\text{rec}}^\ell = 0.5$. Indeed, by increasing the R_{rec}^ℓ value, more photons are recombined with the leptons and consequently the migration of events away from the reconstructed Z peak is reduced. This effect is negligible for the “inclusive” case because the $m(\ell^+\ell^-)$ cut is set far below the Z peak.

Even with the presence of the $m(\ell^+\ell^-)$ cut, NLO_{QCD} results at FO and matched to PS_{QCD} are compatible within the statistical error, which is at the permille level. Moving to the PS_{QCD+QED} predictions, in the case of “inclusive” results the differences with the PS_{QCD} case and among different R_{rec}^ℓ choices are within the statistical error. On the contrary, in the case of Z-peak results, the cross section slightly reduces once the photon emission is enabled in the shower and it depends on the value of R_{rec}^ℓ ; it increases by increasing R_{rec}^ℓ . Still, similarly to the FO case at NLO_{QCD+EW} accuracy, the differences are within 5FS QCD scale uncertainties.

By looking only at total rates obtained with the same R_{rec}^ℓ value, it is difficult to determine, especially in the Z-peak case, the source of the difference between the FO NLO_{QCD+EW} predictions and the NLO_{QCD} results matched with PS_{QCD+QED}. In particular, it is not clear if this difference originates from the multiple emission of photons, which is only present in PS_{QCD+QED}, or the purely weak part of the NLO corrections, which is only included in the

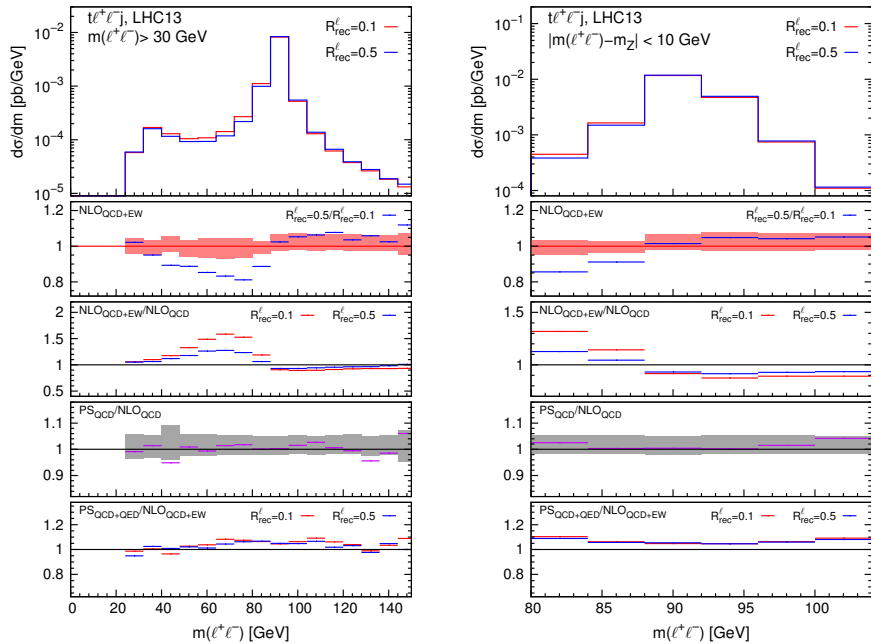


Figure 9: The $m(\ell^+\ell^-)$ distribution in $t\ell^+\ell^-j$ production in the “inclusive” (left) and Z -peak (right) range for different recombination parameters. See the main text for details.

NLO_{QCD+EW} predictions. In order to better understand this issue, it is instructive to repeat the same comparison at the differential level, in particular for the $m(\ell^+\ell^-)$ distribution, which is highly sensitive to FSR QED radiation, as shown in Fig. 8.

In the plots of Fig. 9 we compare $m(\ell^+\ell^-)$ predictions for different R_{rec}^ℓ values, for the “inclusive” case (left) and the Z -peak one (right). In fact, in this figure, the right plot is a zoomed version and with smaller bins of the one on the left. In the main panel, we show results at FO NLO_{QCD+EW} accuracy, for $R_{\text{rec}}^\ell = 0.5$ and $R_{\text{rec}}^\ell = 0.1$. In the first inset we show the ratio of these two different results, together with scale uncertainties for the latter, again in the 5FS. In the second inset we show the NLO_{QCD+EW}/NLO_{QCD} ratio, for both R_{rec}^ℓ values. In the third and fourth inset, shower effects are compared to the fixed-order calculation. In particular, in the third, we show the ratio of NLO_{QCD} predictions matched with PS_{QCD} and at FO, which does not depend on R_{rec}^ℓ , while in the fourth we show the ratio of NLO_{QCD} predictions matched with PS_{QCD+QED} and NLO_{QCD+EW} at FO, again for both R_{rec}^ℓ values.

The first comment on plots of Fig. 9 is that the migration of events to lower $m(\ell^+\ell^-)$ values depends on the R_{rec}^ℓ value, with a much smaller migration for $R_{\text{rec}}^\ell = 0.5$, as can be seen in the first and second insets. However, this dependence is almost identical in the case of FO NLO_{QCD+EW} predictions or NLO_{QCD} ones matched with a PS_{QCD+QED} shower. In fact, the results obtained with these two different simulations are very similar in shape (differences are at the 5–10% level for the normalisation) also close to the Z resonance, as can be seen in the fourth inset. These differences are mainly induced by electroweak effects, not the QCD ones. Indeed, as can be seen in the fourth insets, the differences between the two aforementioned approximations are larger than the differences between NLO_{QCD} predictions at FO and matched with PS_{QCD}. Thus, the differences between FO NLO_{QCD+EW} predictions and those at NLO_{QCD} accuracy matched with a PS_{QCD+QED} shower that are observed in the fourth insets can originate only from two effects: either the purely weak part of the NLO EW corrections or the emissions of photons beyond the first one, which are not part of the FO NLO EW corrections. Since the ratios in the fourth insets are flat and especially do not depend on the value of R_{rec}^ℓ , the differences between the two approximations have to be mainly induced by purely weak contributions from the FO NLO EW corrections.

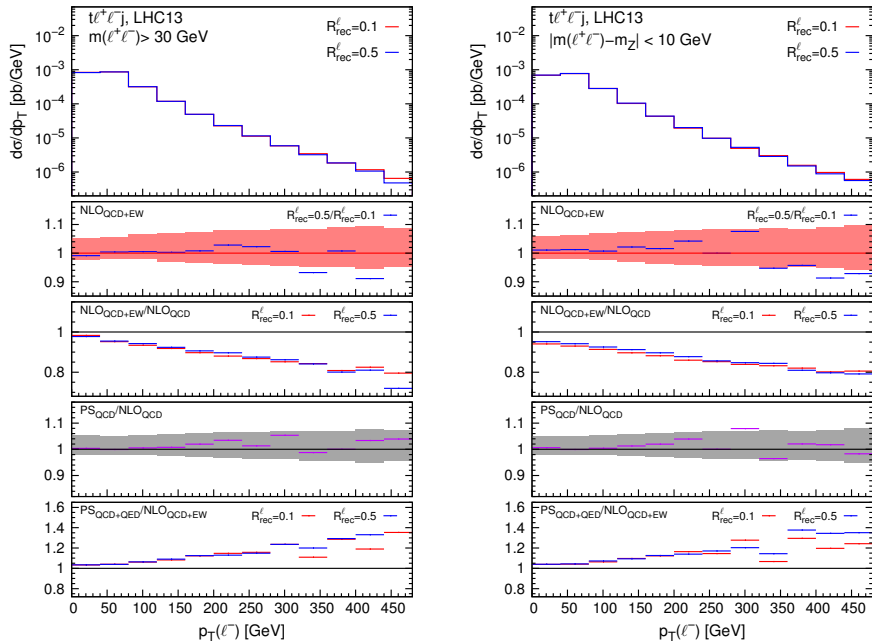


Figure 10: The $p_T(\ell^-)$ distribution in $t\ell^+\ell^-j$ production in the “inclusive” (left) and Z -peak (right) range for different recombination parameters. The layout of the plots is the same of Fig. 9.

Summarising, a shower simulation including QED effects, $\text{PS}_{\text{QCD}+\text{QED}}$, captures very well the effects from NLO EW corrections for the $m(\ell^+\ell^-)$ distribution, within a 5–10% level. This difference is quite flat and is mainly induced by purely weak effects at fixed order. This fact has two consequences. First, also in the case of total rates in Tab. 3 we can safely conclude that the differences observed between $\text{NLO}_{\text{QCD}+\text{EW}}$ and $\text{PS}_{\text{QCD}+\text{QED}}$ results has this origin. Second, by performing a proper matching of the FO $\text{NLO}_{\text{QCD}+\text{EW}}$ calculation and $\text{PS}_{\text{QCD}+\text{QED}}$ simulations, one expects to find a negligible difference w.r.t. the pure FO $\text{NLO}_{\text{QCD}+\text{EW}}$ result.

We want to stress that however the $\text{PS}_{\text{QCD}+\text{QED}}$ parton shower cannot in general capture the impact of NLO EW corrections, *e.g.*, in boosted regimes the purely weak corrections can be large and negative. As an evidence of this behaviour we show in Fig. 10 two plots for the $p_T(\ell^-)$ distribution, using the same layout of those of Fig. 9. At variance with the $m(\ell^+\ell^-)$ distribution, results are almost insensitive to the R_{rec}^ℓ value, but also in this case the inclusion of the QED shower does not have a sizeable effect. The relevance of purely weak corrections can be seen in the last inset. In the tail of the distribution their impact is large and negative and the NLO_{QCD} simulation matched with the $\text{PS}_{\text{QCD}+\text{QED}}$ cannot capture their effect.

In conclusion, whilst a matched simulation at $\text{NLO}_{\text{QCD}+\text{EW}}$ accuracy with $\text{PS}_{\text{QCD}+\text{QED}}$ would further improve the precision, it is not urgently needed for the foreseen accuracy that can be achieved in the next measurements of $t\ell^+\ell^-j$ production, and even more tHj production, at the LHC. We leave this possible improvement to future works.

4 Conclusions

In this paper we have presented and thoroughly discussed the calculation of NLO QCD and EW corrections to the production cross section of a single top (anti)quark in association with either a Higgs (tHj) or a Z boson (tZj) at the LHC. In the context of tZj production, the more realistic $t\ell^+\ell^-j$ final state has also been considered, taking into account off-shell effects and diagrams where the $\ell^+\ell^-$ pair emerges from a photon propagator. The calculation has been

performed in the 5FS via the public version of the code `MADGRAPH5_AMC@NLO` and we have carefully analysed the comparison with predictions obtained in the 4FS in order to estimate the uncertainty due to the flavour-scheme choice. In our calculation, in order to be closer to the experimental measurements, we do not select a specific production mode (t -channel, s -channel or tW associated production with subsequent hadronic W -boson decays). Moreover, the separation of the different production modes is not properly defined at NLO EW accuracy and in general at higher orders. For this reason, the comparison of 4FS and 5FS predictions and in turn the estimation of the flavour-scheme uncertainty is not trivial. To this purpose, we have devised and motivated in detail a strategy, denoted in the text as $5\text{FS}_{4-5}^{\text{scale}}$, where the central value is the one given by the 5FS prediction, either at NLO_{QCD} or $\text{NLO}_{\text{QCD+EW}}$ accuracy, while the relative scale+flavour-scheme uncertainty band is given by the envelope of the 5FS and 4FS scale uncertainties of NLO_{QCD} predictions from t -channel only contributions. Our best predictions, namely at $\text{NLO}_{\text{QCD+EW}}$ accuracy in the $5\text{FS}_{4-5}^{\text{scale}}$, for the LHC at the collision energy of 13 TeV are

$$\begin{aligned}\sigma(tHj) &= 82.2 \text{ fb} \begin{matrix} + 7.2\% \\ -10.9\% \end{matrix} \text{ (scale + flavour)} \begin{matrix} +0.6\% \\ -0.6\% \end{matrix} \text{ (PDFs)}, \\ \sigma(tZj) &= 904 \text{ fb} \begin{matrix} + 5.5\% \\ -11.1\% \end{matrix} \text{ (scale + flavour)} \begin{matrix} +0.4\% \\ -0.4\% \end{matrix} \text{ (PDFs)}, \\ \sigma(t\ell^+\ell^-j) &= 89.6 \text{ fb} \begin{matrix} + 5.6\% \\ -10.4\% \end{matrix} \text{ (scale + flavour)} \begin{matrix} +0.4\% \\ -0.4\% \end{matrix} \text{ (PDFs)} \quad \text{for } m(\ell^+\ell^-) > 30 \text{ GeV}, \\ \sigma(t\ell^+\ell^-j) &= 77.2 \text{ fb} \begin{matrix} + 5.6\% \\ -11.3\% \end{matrix} \text{ (scale + flavour)} \begin{matrix} +0.4\% \\ -0.4\% \end{matrix} \text{ (PDFs)} \quad \text{for } |m(\ell^+\ell^-) - m_Z| < 10 \text{ GeV},\end{aligned}$$

where each cross section refers to the sum of the case of a top quark and a top antiquark.

The size of the EW corrections is for all four cases smaller than the scale+flavour uncertainties, which is purely of QCD origin. However, if we had considered the 5FS only, they would have been (much) larger than the scale uncertainties, with the exception of $\sigma(tZj)$. A similar pattern has been observed also for differential distributions. On the other hand, for large transverse momenta (~ 300 GeV) of the light jet or the heavy boson, the EW corrections are as large as (tHj and tZj) or even larger ($t\ell^+\ell^-j$, especially by requiring $|m(\ell^+\ell^-) - m_Z| < 10$ GeV) than the scale+flavour uncertainties in the $5\text{FS}_{4-5}^{\text{scale}}$.

Finally, in the case of $t\ell^+\ell^-j$ production, we have also compared fixed-order predictions at $\text{NLO}_{\text{QCD+EW}}$ accuracy with NLO_{QCD} predictions matched with $\text{PS}_{\text{QCD+QED}}$, a parton shower simulation including also multiple photon emissions. First, we have verified that in both approximations total rates are almost insensitive to the photon-lepton recombination parameter. Second, we have shown that the $m(\ell^+\ell^-)$ spectrum at $\text{NLO}_{\text{QCD+EW}}$ accuracy can be very well reproduced by the NLO_{QCD} calculation matched with $\text{PS}_{\text{QCD+QED}}$. Differences are quite flat and at the 5–10% level and they originate from the purely weak component of NLO EW corrections, which also explains the differences observed for total rates in the two different approximations. On the contrary, the corrections induced by the $\text{PS}_{\text{QCD+QED}}$ beyond the first photon emission, which is already included in the $\text{NLO}_{\text{QCD+EW}}$ calculation, are negligible. Finally, we have explicitly shown that for other lepton-based observables, such as the $p_T(\ell^-)$ distributions, the purely weak component of NLO EW corrections can be non-negligible and therefore the $\text{PS}_{\text{QCD+QED}}$ cannot correctly reproduce the $\text{NLO}_{\text{QCD+EW}}$ predictions.

Acknowledgements

We want to thank Rikkert Frederix and Marco Zaro for interesting discussions and suggestions. We are grateful to the developers of `MADGRAPH5_AMC@NLO` for the long-standing collaboration and for discussions. The work of D. P. is supported by the Deutsche Forschungsgemeinschaft (DFG) under Germany’s Excellence Strategy - EXC 2121 “Quantum Universe” - 390833306. The work of I.T. is supported by the Swedish Research Council under contract number 2016-05996.

References

- [1] CMS Collaboration, A. M. Sirunyan *et al.*, “Observation of Single Top Quark Production in Association with a Z Boson in Proton-Proton Collisions at $\sqrt{s} = 13$ TeV”, *Phys. Rev. Lett.* **122** no. 13, (2019) 132003, [arXiv:1812.05900 \[hep-ex\]](#).
- [2] CMS Collaboration, A. M. Sirunyan *et al.*, “Measurement of the associated production of a single top quark and a Z boson in pp collisions at $\sqrt{s} = 13$ TeV”, *Phys. Lett.* **B779** (2018) 358–384, [arXiv:1712.02825 \[hep-ex\]](#).
- [3] ATLAS Collaboration, M. Aaboud *et al.*, “Measurement of the production cross-section of a single top quark in association with a Z boson in proton-proton collisions at 13 TeV with the ATLAS detector”, *Phys. Lett.* **B780** (2018) 557–577, [arXiv:1710.03659 \[hep-ex\]](#).
- [4] ATLAS Collaboration, G. Aad *et al.*, “Observation of the associated production of a top quark and a Z boson in pp collisions at $\sqrt{s} = 13$ TeV with the ATLAS detector”, [arXiv:2002.07546 \[hep-ex\]](#).
- [5] CMS Collaboration, V. Khachatryan *et al.*, “Search for the associated production of a Higgs boson with a single top quark in proton-proton collisions at $\sqrt{s} = 8$ TeV”, *JHEP* **06** (2016) 177, [arXiv:1509.08159 \[hep-ex\]](#).
- [6] CMS Collaboration, C. Collaboration, “Search for H to $b\bar{b}$ in association with a single top quark as a test of Higgs boson couplings at 13 TeV”,.
- [7] CMS Collaboration, A. M. Sirunyan *et al.*, “Search for associated production of a Higgs boson and a single top quark in proton-proton collisions at $\sqrt{s} = 13$ TeV”, *Phys. Rev.* **D99** no. 9, (2019) 092005, [arXiv:1811.09696 \[hep-ex\]](#).
- [8] F. Maltoni, K. Paul, T. Stelzer, and S. Willenbrock, “Associated production of Higgs and single top at hadron colliders”, *Phys. Rev.* **D64** (2001) 094023, [arXiv:hep-ph/0106293 \[hep-ph\]](#).
- [9] S. Biswas, E. Gabrielli, and B. Mele, “Single top and Higgs associated production as a probe of the Htt coupling sign at the LHC”, *JHEP* **01** (2013) 088, [arXiv:1211.0499 \[hep-ph\]](#).
- [10] M. Farina, C. Grojean, F. Maltoni, E. Salvioni, and A. Thamm, “Lifting degeneracies in Higgs couplings using single top production in association with a Higgs boson”, *JHEP* **05** (2013) 022, [arXiv:1211.3736 \[hep-ph\]](#).
- [11] F. Demartin, F. Maltoni, K. Mawatari, and M. Zaro, “Higgs production in association with a single top quark at the LHC”, *Eur. Phys. J.* **C75** no. 6, (2015) 267, [arXiv:1504.00611 \[hep-ph\]](#).
- [12] C. Degrande, F. Maltoni, K. Mimasu, E. Vryonidou, and C. Zhang, “Single-top associated production with a Z or H boson at the LHC: the SMEFT interpretation”, *JHEP* **10** (2018) 005, [arXiv:1804.07773 \[hep-ph\]](#).
- [13] J. Campbell, R. K. Ellis, and R. Röntsch, “Single top production in association with a Z boson at the LHC”, *Phys. Rev.* **D87** (2013) 114006, [arXiv:1302.3856 \[hep-ph\]](#).

- [14] S. Amoroso *et al.*, “Les Houches 2019: Physics at TeV Colliders: Standard Model Working Group Report”, in *11th Les Houches Workshop on Physics at TeV Colliders: PhysTeV Les Houches (PhysTeV 2019) Les Houches, France, June 10-28, 2019*. 2020. [arXiv:2003.01700 \[hep-ph\]](#).
- [15] J. Alwall, R. Frederix, S. Frixione, V. Hirschi, F. Maltoni, O. Mattelaer, H. S. Shao, T. Stelzer, P. Torrielli, and M. Zaro, “The automated computation of tree-level and next-to-leading order differential cross sections, and their matching to parton shower simulations”, *JHEP* **07** (2014) 079, [arXiv:1405.0301 \[hep-ph\]](#).
- [16] R. Frederix, S. Frixione, V. Hirschi, D. Pagani, H. S. Shao, and M. Zaro, “The automation of next-to-leading order electroweak calculations”, *JHEP* **07** (2018) 185, [arXiv:1804.10017 \[hep-ph\]](#).
- [17] S. Frixione, V. Hirschi, D. Pagani, H. S. Shao, and M. Zaro, “Weak corrections to Higgs hadroproduction in association with a top-quark pair”, *JHEP* **09** (2014) 065, [arXiv:1407.0823 \[hep-ph\]](#).
- [18] S. Frixione, V. Hirschi, D. Pagani, H. S. Shao, and M. Zaro, “Electroweak and QCD corrections to top-pair hadroproduction in association with heavy bosons”, *JHEP* **06** (2015) 184, [arXiv:1504.03446 \[hep-ph\]](#).
- [19] D. Pagani, I. Tsinikos, and M. Zaro, “The impact of the photon PDF and electroweak corrections on $t\bar{t}$ distributions”, *Eur. Phys. J.* **C76** no. 9, (2016) 479, [arXiv:1606.01915 \[hep-ph\]](#).
- [20] R. Frederix, S. Frixione, V. Hirschi, D. Pagani, H.-S. Shao, and M. Zaro, “The complete NLO corrections to dijet hadroproduction”, *JHEP* **04** (2017) 076, [arXiv:1612.06548 \[hep-ph\]](#).
- [21] M. Czakon, D. Heymes, A. Mitov, D. Pagani, I. Tsinikos, and M. Zaro, “Top-pair production at the LHC through NNLO QCD and NLO EW”, *JHEP* **10** (2017) 186, [arXiv:1705.04105 \[hep-ph\]](#).
- [22] R. Frederix, D. Pagani, and M. Zaro, “Large NLO corrections in $t\bar{t}W^\pm$ and $t\bar{t}\bar{t}$ hadroproduction from supposedly subleading EW contributions”, *JHEP* **02** (2018) 031, [arXiv:1711.02116 \[hep-ph\]](#).
- [23] A. Broggio, A. Ferroglia, R. Frederix, D. Pagani, B. D. Pecjak, and I. Tsinikos, “Top-quark pair hadroproduction in association with a heavy boson at NLO+NNLL including EW corrections”, *JHEP* **08** (2019) 039, [arXiv:1907.04343 \[hep-ph\]](#).
- [24] R. Frederix, D. Pagani, and I. Tsinikos, “Precise predictions for single-top production: the impact of EW corrections and QCD shower on the t -channel signature”, *JHEP* **09** (2019) 122, [arXiv:1907.12586 \[hep-ph\]](#).
- [25] A. Kulesza, L. Motyka, D. Schwartländer, T. Stebel, and V. Theeuwes, “Associated top quark pair production with a heavy boson: differential cross sections at NLO+NNLL accuracy”, [arXiv:2001.03031 \[hep-ph\]](#).
- [26] R. Frederix and I. Tsinikos, “Subleading EW corrections and spin-correlation effects in $t\bar{t}W$ multi-lepton signatures”, [arXiv:2004.09552 \[hep-ph\]](#).
- [27] F. Maltoni, G. Ridolfi, and M. Ubiali, “b-initiated processes at the LHC: a reappraisal”, *JHEP* **07** (2012) 022, [arXiv:1203.6393 \[hep-ph\]](#). [Erratum: *JHEP*04,095(2013)].

- [28] M. Lim, F. Maltoni, G. Ridolfi, and M. Ubiali, “Anatomy of double heavy-quark initiated processes”, *JHEP* **09** (2016) 132, [arXiv:1605.09411 \[hep-ph\]](#).
- [29] R. Frederix, “Top Quark Induced Backgrounds to Higgs Production in the $WW^{(*)} \rightarrow ll\nu\nu$ Decay Channel at Next-to-Leading-Order in QCD”, *Phys. Rev. Lett.* **112** no. 8, (2014) 082002, [arXiv:1311.4893 \[hep-ph\]](#).
- [30] F. Cascioli, S. Kallweit, P. Maierhöfer, and S. Pozzorini, “A unified NLO description of top-pair and associated Wt production”, *Eur. Phys. J.* **C74** no. 3, (2014) 2783, [arXiv:1312.0546 \[hep-ph\]](#).
- [31] T. Ježo, J. M. Lindert, P. Nason, C. Oleari, and S. Pozzorini, “An NLO+PS generator for $t\bar{t}$ and Wt production and decay including non-resonant and interference effects”, *Eur. Phys. J.* **C76** no. 12, (2016) 691, [arXiv:1607.04538 \[hep-ph\]](#).
- [32] S. Frixione, E. Laenen, P. Motylinski, B. R. Webber, and C. D. White, “Single-top hadroproduction in association with a W boson”, *JHEP* **07** (2008) 029, [arXiv:0805.3067 \[hep-ph\]](#).
- [33] W. Hollik, J. M. Lindert, and D. Pagani, “NLO corrections to squark-squark production and decay at the LHC”, *JHEP* **03** (2013) 139, [arXiv:1207.1071 \[hep-ph\]](#).
- [34] W. Beenakker, R. Hopker, M. Spira, and P. M. Zerwas, “Squark and gluino production at hadron colliders”, *Nucl. Phys.* **B492** (1997) 51–103, [arXiv:hep-ph/9610490 \[hep-ph\]](#).
- [35] R. Gavin, C. Hangst, M. Krämer, M. Mühlleitner, M. Pellen, E. Popenza, and M. Spira, “Matching Squark Pair Production at NLO with Parton Showers”, *JHEP* **10** (2013) 187, [arXiv:1305.4061 \[hep-ph\]](#).
- [36] F. Demartin, B. Maier, F. Maltoni, K. Mawatari, and M. Zaro, “tWH associated production at the LHC”, *Eur. Phys. J.* **C77** no. 1, (2017) 34, [arXiv:1607.05862 \[hep-ph\]](#).
- [37] D. Pagani, H.-S. Shao, and M. Zaro, “RIP $Hb\bar{b}$: How other Higgs production modes conspire to kill a rare signal at the LHC”, [arXiv:2005.10277 \[hep-ph\]](#).
- [38] A. Denner, S. Dittmaier, M. Roth, and D. Wackerroth, “Predictions for all processes $e+e- \rightarrow 4$ fermions + gamma”, *Nucl. Phys. B* **560** (1999) 33–65, [arXiv:hep-ph/9904472](#).
- [39] A. Denner, S. Dittmaier, M. Roth, and L. Wieders, “Electroweak corrections to charged-current $e+e- \rightarrow 4$ fermion processes: Technical details and further results”, *Nucl. Phys. B* **724** (2005) 247–294, [arXiv:hep-ph/0505042](#). [Erratum: *Nucl.Phys.B* 854, 504–507 (2012)].
- [40] **NNPDF** Collaboration, R. D. Ball *et al.*, “Parton distributions for the LHC Run II”, *JHEP* **04** (2015) 040, [arXiv:1410.8849 \[hep-ph\]](#).
- [41] V. Bertone and S. Carrazza, “Combining NNPDF3.0 and NNPDF2.3QED through the APFEL evolution code”, *PoS DIS2016* (2016) 031, [arXiv:1606.07130 \[hep-ph\]](#).
- [42] **NNPDF** Collaboration, R. D. Ball *et al.*, “Parton distributions from high-precision collider data”, *Eur. Phys. J.* **C77** no. 10, (2017) 663, [arXiv:1706.00428 \[hep-ph\]](#).
- [43] **NNPDF** Collaboration, V. Bertone, S. Carrazza, N. P. Hartland, and J. Rojo, “Illuminating the photon content of the proton within a global PDF analysis”, *SciPost Phys.* **5** no. 1, (2018) 008, [arXiv:1712.07053 \[hep-ph\]](#).

- [44] L. A. Harland-Lang, A. D. Martin, P. Motylinski, and R. S. Thorne, “Parton distributions in the LHC era: MMHT 2014 PDFs”, *Eur. Phys. J. C* **75** no. 5, (2015) 204, [arXiv:1412.3989 \[hep-ph\]](#).
- [45] L. A. Harland-Lang, A. D. Martin, R. Nathvani, and R. S. Thorne, “Ad Lucem: QED Parton Distribution Functions in the MMHT Framework”, *Eur. Phys. J. C* **79** no. 10, (2019) 811, [arXiv:1907.02750 \[hep-ph\]](#).
- [46] A. Manohar, P. Nason, G. P. Salam, and G. Zanderighi, “How bright is the proton? A precise determination of the photon parton distribution function”, *Phys. Rev. Lett.* **117** no. 24, (2016) 242002, [arXiv:1607.04266 \[hep-ph\]](#).
- [47] A. V. Manohar, P. Nason, G. P. Salam, and G. Zanderighi, “The Photon Content of the Proton”, *JHEP* **12** (2017) 046, [arXiv:1708.01256 \[hep-ph\]](#).
- [48] R. D. Ball, V. Bertone, F. Cerutti, L. Del Debbio, S. Forte, A. Guffanti, J. I. Latorre, J. Rojo, and M. Ubiali, “Impact of Heavy Quark Masses on Parton Distributions and LHC Phenomenology”, *Nucl. Phys. B* **849** (2011) 296–363, [arXiv:1101.1300 \[hep-ph\]](#).
- [49] M. Cacciari, G. P. Salam, and G. Soyez, “The anti- k_t jet clustering algorithm”, *JHEP* **04** (2008) 063, [arXiv:0802.1189 \[hep-ph\]](#).
- [50] M. Cacciari, G. P. Salam, and G. Soyez, “FastJet User Manual”, *Eur. Phys. J. C* **72** (2012) 1896, [arXiv:1111.6097 \[hep-ph\]](#).
- [51] S. Frixione, Z. Kunszt, and A. Signer, “Three jet cross-sections to next-to-leading order”, *Nucl. Phys. B* **467** (1996) 399–442, [arXiv:hep-ph/9512328 \[hep-ph\]](#).
- [52] S. Frixione, “A General approach to jet cross-sections in QCD”, *Nucl. Phys. B* **507** (1997) 295–314, [arXiv:hep-ph/9706545 \[hep-ph\]](#).
- [53] R. Frederix, S. Frixione, F. Maltoni, and T. Stelzer, “Automation of next-to-leading order computations in QCD: The FKS subtraction”, *JHEP* **10** (2009) 003, [arXiv:0908.4272 \[hep-ph\]](#).
- [54] R. Frederix, S. Frixione, A. S. Papanastasiou, S. Prestel, and P. Torrielli, “Off-shell single-top production at NLO matched to parton showers”, *JHEP* **06** (2016) 027, [arXiv:1603.01178 \[hep-ph\]](#).
- [55] G. Ossola, C. G. Papadopoulos, and R. Pittau, “Reducing full one-loop amplitudes to scalar integrals at the integrand level”, *Nucl. Phys. B* **763** (2007) 147–169, [arXiv:hep-ph/0609007 \[hep-ph\]](#).
- [56] P. Mastrolia, E. Mirabella, and T. Peraro, “Integrand reduction of one-loop scattering amplitudes through Laurent series expansion”, *JHEP* **06** (2012) 095, [arXiv:1203.0291 \[hep-ph\]](#). [Erratum: *JHEP*11,128(2012)].
- [57] G. Passarino and M. J. G. Veltman, “One Loop Corrections for $e^+ e^-$ Annihilation Into $\mu^+ \mu^-$ in the Weinberg Model”, *Nucl. Phys. B* **160** (1979) 151–207.
- [58] A. I. Davydychev, “A Simple formula for reducing Feynman diagrams to scalar integrals”, *Phys. Lett. B* **263** (1991) 107–111.
- [59] A. Denner and S. Dittmaier, “Reduction schemes for one-loop tensor integrals”, *Nucl. Phys. B* **734** (2006) 62–115, [arXiv:hep-ph/0509141 \[hep-ph\]](#).

- [60] V. Hirschi, R. Frederix, S. Frixione, M. V. Garzelli, F. Maltoni, and R. Pittau, “Automation of one-loop QCD corrections”, *JHEP* **05** (2011) 044, [arXiv:1103.0621 \[hep-ph\]](#).
- [61] G. Ossola, C. G. Papadopoulos, and R. Pittau, “CutTools: A Program implementing the OPP reduction method to compute one-loop amplitudes”, *JHEP* **03** (2008) 042, [arXiv:0711.3596 \[hep-ph\]](#).
- [62] T. Peraro, “Ninja: Automated Integrand Reduction via Laurent Expansion for One-Loop Amplitudes”, *Comput. Phys. Commun.* **185** (2014) 2771–2797, [arXiv:1403.1229 \[hep-ph\]](#).
- [63] V. Hirschi and T. Peraro, “Tensor integrand reduction via Laurent expansion”, *JHEP* **06** (2016) 060, [arXiv:1604.01363 \[hep-ph\]](#).
- [64] A. Denner, S. Dittmaier, and L. Hofer, “Collier: a fortran-based Complex One-Loop Library in Extended Regularizations”, *Comput. Phys. Commun.* **212** (2017) 220–238, [arXiv:1604.06792 \[hep-ph\]](#).
- [65] F. Cascioli, P. Maierhofer, and S. Pozzorini, “Scattering Amplitudes with Open Loops”, *Phys. Rev. Lett.* **108** (2012) 111601, [arXiv:1111.5206 \[hep-ph\]](#).
- [66] J. M. Campbell, R. Frederix, F. Maltoni, and F. Tramontano, “Next-to-Leading-Order Predictions for t-Channel Single-Top Production at Hadron Colliders”, *Phys. Rev. Lett.* **102** (2009) 182003, [arXiv:0903.0005 \[hep-ph\]](#).
- [67] T. Sjöstrand, S. Mrenna, and P. Z. Skands, “A Brief Introduction to PYTHIA 8.1”, *Comput. Phys. Commun.* **178** (2008) 852–867, [arXiv:0710.3820 \[hep-ph\]](#).
- [68] T. Sjöstrand, S. Ask, J. R. Christiansen, R. Corke, N. Desai, P. Ilten, S. Mrenna, S. Prestel, C. O. Rasmussen, and P. Z. Skands, “An Introduction to PYTHIA 8.2”, *Comput. Phys. Commun.* **191** (2015) 159–177, [arXiv:1410.3012 \[hep-ph\]](#).
- [69] S. Frixione and B. R. Webber, “Matching NLO QCD computations and parton shower simulations”, *JHEP* **06** (2002) 029, [arXiv:hep-ph/0204244](#).